Desalination 613 (2025) 119052

Contents lists available at ScienceDirect

Desalination

journal homepage: www.elsevier.com/locate/desal

Pilot scale production of $Mg(OH)_2$ compounds from a real industrial reverse osmosis desalination brine

Lorenzo Ventimiglia [a], Fabrizio Vassallo [d], Giuseppe Lo Burgio [b], Antonino Campione [b,*], Laura Cammilli [c], Paolo Vicario [c], Giuseppe Battaglia [a,*], Fabrizio Vicari [d], Andrea Cipollina [a], Alessandro Tamburini [a], Giorgio Micale [a]

[a] Università degli studi di Palermo, Dipartimento di Ingegneria, Viale delle Scienze, 90128 Palermo, Italy
[b] SUEZ International, 4 Pl. de la Pyramide, 92800 Puteaux, France
[c] SUEZ Italy S.p.a, Via Benigno Crespi, 57, 20159 Milano, Italy
[d] ResourSEAs SrL, Via Notarbartolo n. 38, 90141 Palermo, Italy

HIGHLIGHTS

- $Mg(OH)_2$ was produced at a semi-industrial scale from a RO desalination brine.
- The MF-PFR prototype ensured an effective control of the process.
- $Mg(OH)_2$ solids purity increased from ~94 % to ~98 % after bicarbonate removal.
- pH and reactor hydrodynamics affected $Mg(OH)_2$ suspensions/particles features.

GRAPHICAL ABSTRACT

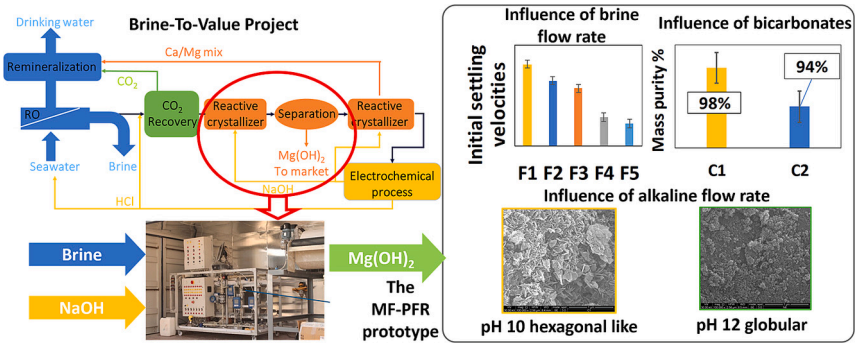

ARTICLE INFO

Keywords:
Desalination
Magnesium hydroxide
Mineral recovery
Pilot scale
Brine mining

ABSTRACT

Brine valorisation technologies have gained substantial interest in the last decade, particularly with respect to the recovery of valuable minerals within integrated schemes. Within this context, several studies have investigated at the laboratory scale the extraction from brines of magnesium hydroxide, $Mg(OH)_2$, a compound widely adopted in several industrial fields. The present work aims at thoroughly assessing, for the first time, the synthesis of $Mg(OH)_2$ from a real industrial reverse osmosis desalination brine at a semi-industrial scale. The brine produced by the industrial seawater reverse osmosis plant installed on the island of Lampedusa was treated in situ by adopting a pilot-scale Multi Feed Plug Flow Reactor with and without specific pre-treatments to enhance the product purity. High-purity (>98 %) values for the $Mg(OH)_2$ solids were achieved; the higher the reaction pH, the higher the Mg^{2+} conversion; settling and filtration features exhibited a maximum rate at pH 11.2, while the lower the brine flow rate the higher the settling and filtration properties of $Mg(OH)_2$ suspensions. Finally, an economic analysis of the $Mg(OH)_2$ production scheme showed the feasibility of the proposed approach, highlighting the large potential for this brine valorisation strategy.

* Corresponding authors.
E-mail addresses: antonino.campione@suez.com (A. Campione), giuseppe.battaglia03@unipa.it (G. Battaglia).

https://doi.org/10.1016/j.desal.2025.119052
Received 14 April 2025; Received in revised form 19 May 2025; Accepted 21 May 2025
Available online 22 May 2025

1. Introduction

Today, water stress and water scarcity are two ever-expanding challenges [1,2]. Water stress is related to a higher water demand than the available one, while water scarcity concerns either the lack of water sources in specific geographical areas, e.g. deserts or isolated islands (physical water scarcity), or the mismanagement of available supplies (economic water scarcity) [3]. One opportunity to face these problems is the production of drinking water from seawater through desalination technologies. To date, every day 95 million cubic meters of drinking water are produced from seawater [4], of which ~69 % are provided by reverse osmosis (RO) technology [4]. Two aqueous streams are generated in RO units: (i) the permeate, namely a water stream poor in salts that requires to be re-mineralized if used for drinking water purposes, and a retentate/brine, which is a saline solution that has a salinity about twice that of the treated seawater. So far, brines have been considered as rejects, thus being, in most of cases, disposed back into the sea. On the other hand, seawater and, thus, seawater desalination brines, contain almost all the elements of the periodic table [5]. These solutions are, therefore, fruitful sources of chemicals, fresh water and added-value compounds. Magnesium is one of the most economically advantageous elements to be recovered from brines [6–8]. Magnesium is the third most abundant element in reverse osmosis brines after chlorine and sodium, with an average concentration of ~2.4 g/L. Magnesium and its compounds are extensively adopted in several industrial applications [9]. Moreover, they have a crucial economic value for the European Union (EU) due to their geopolitical supply risk. As a matter of fact, the EU has included magnesium among the 30 "critical raw materials" for the EU's economy [10,11]. Among the others, magnesium hydroxide, $Mg(OH)_2$, is a white odourless compound extensively adopted as a flame-retardant filler in plastic materials, as an acid neutralizer in wastewater treatment and as a precursor for magnesium oxide catalysts [12,13]. Commercial grade $Mg(OH)_2$ powders must have a purity higher than 95 % [14]. $Mg(OH)_2$ powders should have a purity >98 % for flame retardant and pharmaceutical applications [15]. Low purity slurries, for wastewater treatment, can have a price of ~400–500 $/ton-$Mg(OH)_2$ [16], while solids with high purity can reach values of 1000–1500 $/ton-$Mg(OH)_2$ [17–19]. These latter values can even increase if $Mg(OH)_2$ solids comply with surface area requirements for flame retard applications. In the last 30 years, the recovery of $Mg(OH)_2$ from unconventional sources has attracted the interest of several researchers and industrials. At a laboratory scale, Turek and Gnot [20] investigated the recovery of Mg ions in the form of $Mg(OH)_2$ solids from coal mine brines (concentration of Mg^{2+} of 2.8 g/L), assessing the influence of the reaction temperature, the stirring speed and the reaction time. Sodium hydroxide solutions were employed as the alkaline reagent. Settling and filtration rates were found to be in the range of 70–170 mm/h and 3–9 kg/m^2 h, respectively. Dong et al. [21] studied the recovery of magnesium hydroxide from rejected brines collected from a local desalination plant in Singapore. The authors adopted different amounts of ammonium hydroxide, NH_4OH, as a reactant agent, to optimize the Mg^{2+} recovery limiting the co-precipitation of Ca^{2+}. An optimum NH_4OH/Mg^{2+} ratio of 6 resulted in a high Mg^{2+} recovery, minimizing Ca-based impurities at the same time, being the purity of $Mg(OH)_2$ solids ~93.5 %.

Gong et al. [14] employed a slaked 83 % wt calcium oxide (quicklime) solution to precipitate magnesium hydroxide from seawater brine produced in a desalination plant in Perth, Australia. The purity of the solids was found to be ~60 % due to the co-precipitation of calcium species, such as calcium carbonate ($CaCO_3$) and calcium sulfate ($CaSO_4$). A wet screening of the lime slurry allowed the purity of $Mg(OH)_2$ powders to be enhanced up to 91 %.

At a pilot scale, Morgante et al. [22] studied the influence of several parameters on the $Mg(OH)_2$ precipitation process from synthetic Mg^{2+} solutions (5.83 g/L and 24.3 g/L) by adopting a pilot-scale Multi Feed Plug Flow Reactor. The recirculation strategy of part of the produced $Mg(OH)_2$ suspensions was found to improve their settling and filtration characteristics. Morgante et al. [23] also proved the possible integration of a similar pilot-scale crystallizer in an integrated treatment chain for the sustainable production of freshwater and minerals from desalination brines. In this case, the retentate solution (concentrated in bivalent ions, Mg^{2+} 4.65 g/L) of a nanofiltration unit, treating a desalination brine, was fed to the $Mg(OH)_2$ crystallizer. $Mg(OH)_2$ solids with an average purity of around 94 % were obtained. Battaglia et al. [24] extensively characterized the $Mg(OH)_2$ powders produced from real saltworks bitterns (Mg^{2+} 49 g/L) at a pilot scale. High pH values guaranteed high Mg^{2+} recovery and solids purities, i.e. > 98 %, with boron content complying with market requirements, however, filtration characteristics were worsened due to the lyosorption phenomenon.

In order to increase the low purity of $Mg(OH)_2$ powders synthesized from seawater brines (90–96 %), several approaches have been proposed [25]. Sano et al. [26] investigated the continuous recovery of magnesium from seawater brines by adopting an electrodialysis stack. The authors applied deaeration methods (both the acid supply or the boiling) to remove carbon dioxide producing $Mg(OH)_2$ solids with a purity up to 99 %. Vassallo et al. [27] treated an exhausted brine of the regeneration stage of ion exchange resins in a softening water industry. The brine was acidified at a pH value below 4, to convert bicarbonates into carbon dioxide, which was further removed by adopting a stripping unit. The purity of synthesized $Mg(OH)_2$ solids was found to increase from 91 % to 99 %. Molinari et al. [28] treated synthetic desalination brines with sodium citrate ($Na_3C_6H_5O_7$), carbonate (Na_2CO_3) and hydrogencarbonate ($NaHCO_3$) to remove Ca ions. A Ca^{2+} removal efficiency higher than 90 % was obtained at 60 °C and controlled pH when using $NaHCO_3$ with an Mg^{2+} loss below 7 %. Ventimiglia et al. [29] investigated the possible application of evaporative ponds as a pre-treatment of synthetic seawater desalination brines. Calcium ions precipitated in the evaporation ponds allowed the purity of $Mg(OH)_2$ solids to be enhanced from ~90 % to values higher than 99 %.

Although, the synthesis of $Mg(OH)_2$ solids has been analysed both at laboratory- and pilot- scales, for the best of authors' knowledge, there are no works dealing with $Mg(OH)_2$ production from real seawater reverse osmosis brines (without any concentration pre-treatment) at industrial or semi-industrial scale. The present work aims at filling this gap by thoroughly assessing, for the first time, the sustainable production of high-purity $Mg(OH)_2$ compounds from industrial RO desalination brines at a preindustrial scale. Activities were carried out in the framework of the " Brine-To-Value " project [30], an industry-driven project (involving the University of Palermo, SUEZ international, SUEZ Italy, and ResourSEAS). The aim of the project is the valorization of desalination brines to produce marketable magnesium hydroxide powders and a drinkable permeate stream by adopting in situ generated chemicals. The patented [30] conceptual design scheme of the "Brine-To-Value" project is shown in Fig. 1.

The brine stream from the seawater reverse osmosis (SWRO) plant is acidified by adding a hydrochloric acid, HCl, solution and treated in a dedicated stripping column for CO_2 removal. The brine, poor in bicarbonate ions, is fed to a crystallizer to produce highly pure magnesium hydroxide solids via addition of NaOH solutions. After solids separation, the clarified solution is fed into a second crystallization unit for the production of a mix of calcium and magnesium minerals that could be employed for the remineralization of the permeate stream. The clarified solution, from the second crystallization unit, is further processed in an electrodialysis unit with bipolar membranes (EDBM) to produce in situ the HCl and NaOH solutions required by the process [31]. The use of in-situ EDBM units have different advantages: i) further valorization of waste saline streams, with potential for reaching fully circular operating schemes; ii) the production of targeted alkaline and acidic solution at the required concentration, thus avoiding dissolution/dilution steps, often characterized by higher risks for the operators and equipment; iii) lower cost of the chemicals obtained, due to the lower targeted concentrations and lack of transportation costs; iv) a partial desalination of the waste saline stream that allows for a full recirculation of this latter in the

SWRO unit, thus enhancing the overall process water recovery and sustainability. As far as the feasibility of the EDBM process is concerned, it can be somewhat affected by the composition of the saline streams used as a feed brine. A prerequisite for optimal operation is to guarantee a molar flowrate of salt arriving with this brine higher than the molar flow rate of NaOH or HCl products. Virruso et al. [31] have shown how the volume ratio between the saline feed and the alkaline/acidic solution has an impact on the system performance, with lower energy consumption and larger productivities when an "excess" of saline solution of about 50 % is guaranteed (assuming inlet salt molar concentration equal to the outlet NaOH one). As an example, in the present case scenarios, a brine flow rate exiting from the MF-PFR reactor of 130 L/h at a NaCl concentration of about 0.6 M is generated and available to feed the EDBM unit, while the target capacity of this latter is around 30 L/h of NaOH solution at 0.5 M, thus guaranteeing a molar ratio between salt available and product to generate higher than 5. The "Brine-To-Value" project scheme was implemented in the island of Lampedusa to treat a real reverse osmosis desalination brine. In particular, $Mg(OH)_2$ solids were produced by adopting the Multi Feed Plug Flow Reactor, MF-PFR, prototype, which has been designed by ResourSEAs and the University of Palermo [32]. The influence of (i) brine pre-treatment to remove bicarbonate species, (ii) reaction pH and (iii) brine flow rate was assessed on the (i) settling and filtration rates of produced $Mg(OH)_2$ suspensions, (ii) purity of $Mg(OH)_2$ powders, (iii) content of micro and macro elements in $Mg(OH)_2$ powders, and (iv) morphology of the solids. In addition, a techno-economics analysis was carried out to investigate the economics feasibility of the process with and without the pre-treatment step of inorganic carbon removal.

2. Materials and methods

2.1. The pilot unit

The pilot scale Multi-Feed Plug Flow reactor, MF-PFR, was adopted to synthesize $Mg(OH)_2$ solids from seawater desalination brines. The MF-PFR crystallizer is a tubular unit made of two coaxial tubes [32]. A picture of the MF-PFR pilot unit and a schematic representation of the $Mg(OH)_2$ precipitation process occurring inside the reactor are shown in Fig. 2.a and b, respectively.

The brine was fed in the inner tube, while the NaOH solution flowed in the annular section. The brine was then injected into the alkaline compartment through nozzles distributed along the reactor length. In the reactor, the $Mg(OH)_2$ precipitation process took place according to Eq. (1):

$$Mg^{2+}(aq) + 2{\cdot}OH^{-}(aq) = Mg(OH)_2(s)\downarrow \quad (1)$$

A part of the produced $Mg(OH)_2$ suspension was recirculated back to the inlet section to (i) enhance the conversion of Mg^{2+} into $Mg(OH)_2$ solids and (ii) improve settling and filtration features of produced suspensions [22]. It should also be noted that, the multiple injection of the brine in the annular section allowed the supersaturation level in the reaction environment to be well controlled, ensuring, at the same time, a well mixing of the reagents. These two parameters are crucial to avoid the nucleation of tiny particles characterized by poor settling and filtration characteristics. In addition, the accurate control of supersaturation and mixing in the reactor allows the reactor volume to be minimized and, thanks to the tubular geometry, similar arrangements of high-pressure RO module stacks to be adopted.

The crystallizer requires some auxiliary devises: two tanks for reagents storage, namely NaOH and brine solutions; a settling tank for $Mg(OH)_2$ suspensions collection; fluid driving pumps and a monitoring/control system. The brine and the sodium hydroxide streams were fed to the MF-PFR crystallizer by two gear pumps (TEOREMA, mod. FG213 and FG204). The NaOH solution could be pumped inside the crystallizer or pre-diluted by mixing it with the recirculating $Mg(OH)_2$ suspension outcoming from the reactor by adopting a three valve system. In the latter case, the NaOH solution and the recirculating suspension were handled by a magnetically driven centrifugal pump (Schmitt, mod. MPN 150).

A pH meter (Krohne, mod. pH 8320) measured the pH of the $Mg(OH)_2$ suspensions at the outlet of the reactor. The temperature and the conductivity of the brine and of the outlet stream were monitored by conductivity sensors (Krohne mod. OPTISENS IND 1000). Flow rates were measured by magnetic flow meters (Krohne, mod. OPTIFLUX 4100 C and OPTIFLUX 4300 C).

2.2. Saline and alkaline solutions

The feed solution was the brine outcoming a SWRO desalination plant located in the island of Lampedusa producing fresh water for industrial purposes (S.EL.I.S. Lampedusa S.P.A). Table 1 lists the concentration of macro and micro components in the bine and in the

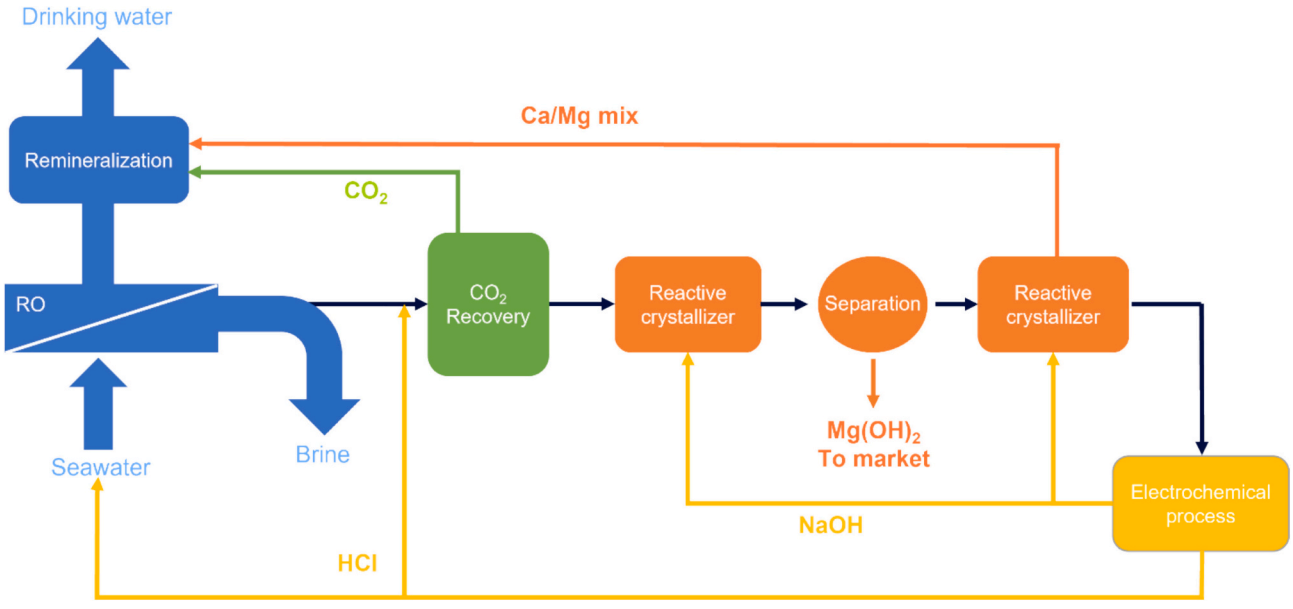

Fig. 1. Overall scheme of the treatment chain of the "Brine-To-Value" project [30].

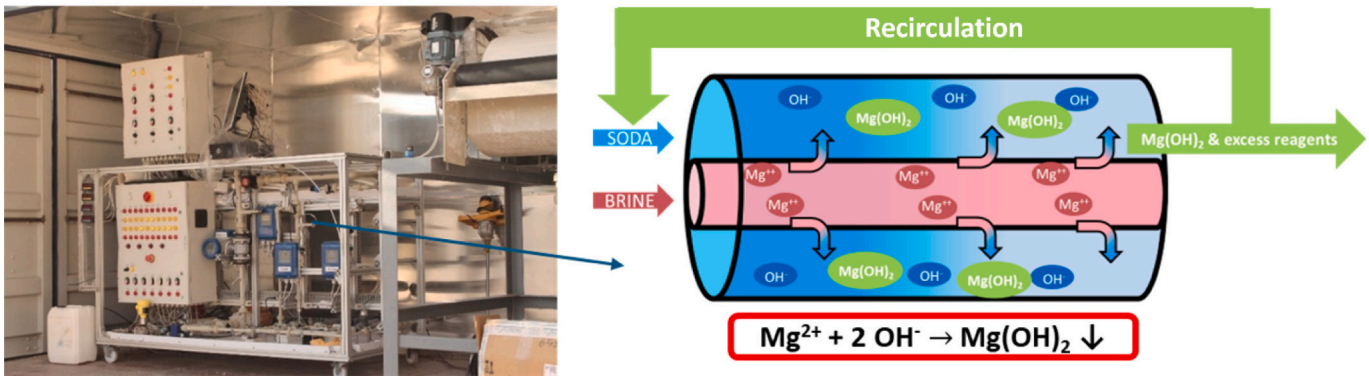

Fig. 2. (a) A picture of MF-PFR pilot unit; (b) a schematic representation of the $Mg(OH)_2$ precipitation process occurring in the MF-PFR crystallizer.

seawater. Turbidity of the brine, measured through the WTW Turb® 750 IR, is also reported. The concentration of sodium, potassium, calcium, magnesium, chloride and sulphate ions was determined by Ion Chromatography technique (IC, Metrohm 882 compact IC plus), the concentration of boron was measured by Inductively Coupled Plasma Optical Emission Spectroscopy (ICP-OES, PerkinElmer Optima 2100 DV), while the content of bicarbonate species was deduced from the total alkalinity of the solution done through titration with sulfuric acid (Honeywell-Fluka, 95–97 % *w*/w), according to the APAT 2010 method (see also ISO 9963-1). The concentration of magnesium and calcium ions was also confirmed through complexometric titration with ethylenediaminetetraacetic acid (EDTA), via APAT 2040 method (see also ISO 6059). The concentration of orthophosphates was determined following the APAT 4110 method (see also ISO 6878).

The alkaline stream was a NaOH solution prepared by diluting a 30 % *w*/w NaOH solution (Chimica Noto, 30 % *w*/w) with the permeate stream (pH ~ 6.1, 400 ± 20 μS/cm) of the RO desalination plant. Hydroxyl ions concentration was measured through acid-base titration, APAT 2010 method (see also ISO 9963-1).

Table 1
Compositions in macro and micro components of the seawater and brine of the industrial desalination plant of Lampedusa (Sicily, Italy).

Macro components	Seawater	Brine	Analytical technique
	Conc. [g/L]	Conc. [g/L]	
Na^+	13 ± 1	18 ± 1	IC[a]
K^+	0.50 ± 0.04	0.60 ± 0.04	IC[a]
Ca^{2+}	0.56 ± 0.05	0.70 ± 0.05	IC[a]/EDTA[b]
Mg^{2+}	1.6 ± 0.1	2.0 ± 0.1	IC[a]/EDTA[b]
Cl^-	22 ± 1	32 ± 1	IC[a]
SO_4^{2-}	3.2 ± 0.1	4.0 ± 0.1	IC[a]

Micro components	Seawater	Brine	Analytical technique
	Conc. [mg/L]	Conc. [mg/L]	
B	–	8.9 ± 1.3	ICP-OES[c]
HCO_3^-	134 ± 2	220 ± 5	Titration
PO_4^{3-} (total)	–	5.2 ± 0.5	APAT 4110

Other characteristics	NTU	NTU
Turbidity	–	0.19

[a] IC, Ion Chromatography.
[b] EDTA, complexometric titration with ethylenediaminetetraacetic acid.
[c] ICP-OES, Inductively Coupled Plasma Optical Emission Spectroscopy.

2.3. Operating conditions

The influence of several parameters was investigated on the characteristics of synthesized $Mg(OH)_2$ suspensions and solids, namely (i) the content of bicarbonates species in the brine, (ii) the reaction pH, and (iii) the feed brine flow rate, as described in Table 2. Note that, as reported in the introduction, the brine, after acidification, was treated in a dedicated stripping column to remove bicarbonates. The bicarbonate (HCO_3^-) removal rate was the ratio between the removed alkalinity (the difference between the bicarbonates content in the brine before and after the treatment) and the alkalinity of the original brine. From a preliminary investigation, a removal rate of 70 % was adopted in all tests as a minimum value for an effective inhibition of $CaCO_3$ co-precipitation.

Tests C evaluated the influence of the brine pre-treatment to remove bicarbonates, following the Brine-To-Value scheme. Tests N were carried out by varying the flow rate of the NaOH solution from 24 L/h up to 47 L/h, thus causing an increase in the reaction pH from 10 to 12.4. Tests F analysed the influence of the feed brine flow rate. In this case, the flow rate of the alkaline stream was also varied in order to keep the reaction pH constant.

Table 2
Summary of the operating conditions adopted in the tests in terms of feed brine flow rate (Q_{Brine}), alkaline flow rate (Q_{NaOH}); reaction pH and bicarbonate (HCO_3^-) removal rate. In all tests, a 0.5 M (2 % *w*/w) sodium hydroxide (NaOH) solution was adopted.

Test	Q_{Brine} [L/h]	Q_{NaOH} [L/h]	pH	% HCO_3^- removal
C1	100 ± 0.06	33 ± 0.06	10.5 ± 0.2	70 ± 5
C2			10.5 ± 0.2	0
N1	100 ± 0.06	24 ± 0.06	10.0 ± 0.3	70 ± 5
N2		28.9 ± 0.06	10.2 ± 0.3	
N3		33 ± 0.06	10.3 ± 0.2	
N4		38 ± 0.06	11.2 ± 0.2	
N5		43 ± 0.06	12.1 ± 0.2	
N6		47 ± 0.06	12.4 ± 0.5	
F1	50 ± 0.06	17 ± 0.06	10.5 ± 0.2	70 ± 5
F2	75 ± 0.06	25.5 ± 0.06	10.5 ± 0.2	
F3	100 ± 0.06	34 ± 0.06	10.5 ± 0.2	
F4	125 ± 0.06	42.5 ± 0.06	10.5 ± 0.2	
F5	150 ± 0.06	51 ± 0.06	10.5 ± 0.2	

2.4. Analytical procedures for the characterization of $Mg(OH)_2$ suspensions and powders

For each test, about 6 L of $Mg(OH)_2$ suspension was collected at the outlet of the reactor. 500 mL were poured in a 500 mL graduated cylinders, Fig. 3.a, while 5 L were stored in a bigger tank, see Fig. 3.b.

The settling process of synthesized $Mg(OH)_2$ suspensions was recorded for ~24 h by following the solid-liquid interface in the 500 mL graduate cylinder, see Fig. 3.a (step A/1). Initial settling velocities were evaluated from settling data following the procedure discussed in the Appendix A.2. After settling, the residual magnesium and calcium concentrations in clarified solutions were assessed by EDTA titration, (step A/2), and then used to calculate the recovery of magnesium (Rec_{Mg}) and calcium (Rec_{Ca}) ions, following Eq. (2):

$$Rec_i = \frac{C_i^{in}/DF - C_i^{final}}{C_i^{in}/DF} \tag{2}$$

where C_i^{in} and C_i^{final} are the concentrations of the *i-th* ions, namely either magnesium or calcium, in the brine and in the clarified solutions, respectively. *DF* is the dilution factor calculated as the ratio between the sum of the flow rate of the alkaline and brine solutions over that of the brine one:

$$DF = \left(\frac{Q_{NaOH} + Q_{brine}}{Q_{brine}}\right) \tag{3}$$

The thickened suspension was washed with RO permeate solutions to dilute soluble compounds entrapped in the concentrated suspension, e.g. sodium chloride, see step A/3. Washing proceeded until the conductivity of the supernatant solution was ~550 μS/cm. After washing, the suspension was suspended again and its settling process was recorded for 24 h, (step A/4). Initial settling velocities were evaluated from settling data following the procedure discussed in the Appendix A.2.

The 5 L samples, stored in a big tank, were washed until the conductivity of the supernatant was ~550 μS/cm, as shown in Fig. 3 (step B/1). Then 100 mL of thickened $Mg(OH)_2$ suspension was filtered (step B/2). Filtration was performed at a fixed vacuum pressure of −0.5 Barg by using a Buchner system and 1.6 μm glass fiber filters of 70 cm diameter (Whatman GF/A grade, GE Healthcare Life Sciences). The filtration rate was computed as Eq. (4):

$$\text{Filtration Rate} = \frac{V_{sol} \cdot M_{TMg(OH)_2}}{t_{filt} \cdot A_{filter}} \cdot FC \tag{4}$$

where, V_{sol} [m^3] is the volume of the filtered suspension, $M_{TMg(OH)_2}$ [kg/m^3] is the magma density of the slurry, A_{filter} [m^2] is the surface of the filter and t_{filt} [h] is the filtration time. *FC* [−] is the concentration factor of the suspension after thickening, namely the ratio between the initial and final volume of the suspension.

The magma density, i.e. the concentration of solids in the suspension, was computed as:

$$M_{TMg(OH)_2} = Rec_{Mg} \cdot \frac{C_{Mg}^{in}}{DF} \cdot PM_{Mg(OH)_2} \tag{5}$$

where $PM_{Mg(OH)_2}$ is the molecular weight of magnesium hydroxide solids, i.e. 58.32 g/mol.

The cake permeability coefficient, θ_{perm}, was also calculated following Eq. (6):

$$\theta_{perm} = \frac{V_{sol}}{t_{filt} \cdot A_{filter} \cdot P_{filt.}} \cdot \left(\frac{V_{sol} \cdot M_{TMg(OH)_2}}{\rho_{cake} \cdot A_{filter}}\right) \cdot FC \tag{6}$$

where ρ_{cake} is the density of the cake [g/L], assumed to be that of the water, and $P_{filt.}$ is the filtration operating pressure [bar]. In Eq. (6) the filtration time $t_{filt.}$ was in minutes, while $M_{TMg(OH)_2}$ was in g/L.

After filtration, the wet cake was weighed and then dried in an oven at 120 °C for about 24 h, (step B/3). The dried cake was also weighted to determine the humidity of the cake as the difference between weights before and after the drying (values reported in Appendix A.4). The dried cake was milled and its purity analysed, step B/4. Specifically, the mass purity of the powder was determined by conducting thermogravimetric analysis (TG or TGA, STA 449 F1 Jupiter analyser, NETZSCH). About 100 mg of $Mg(OH)_2$ powders were loaded in an alumina crucible. In the analysis, samples were heated from 30 °C up to 800 °C at 10 °C/min. A constant flow rate of nitrogen of 20 mL/min was set. Mass purity was calculated following the procedure reported in the Appendix A.3. The cationic purity of the solids was assessed by ion chromatography (IC) (Metrohm model 882 compact IC plus). To this aim, about 150 mg of powders were dissolved in ultrapure hydrochloric acid (Honeywell-Fluka;>30 % for trace analysis). The cationic purity was calculated as:

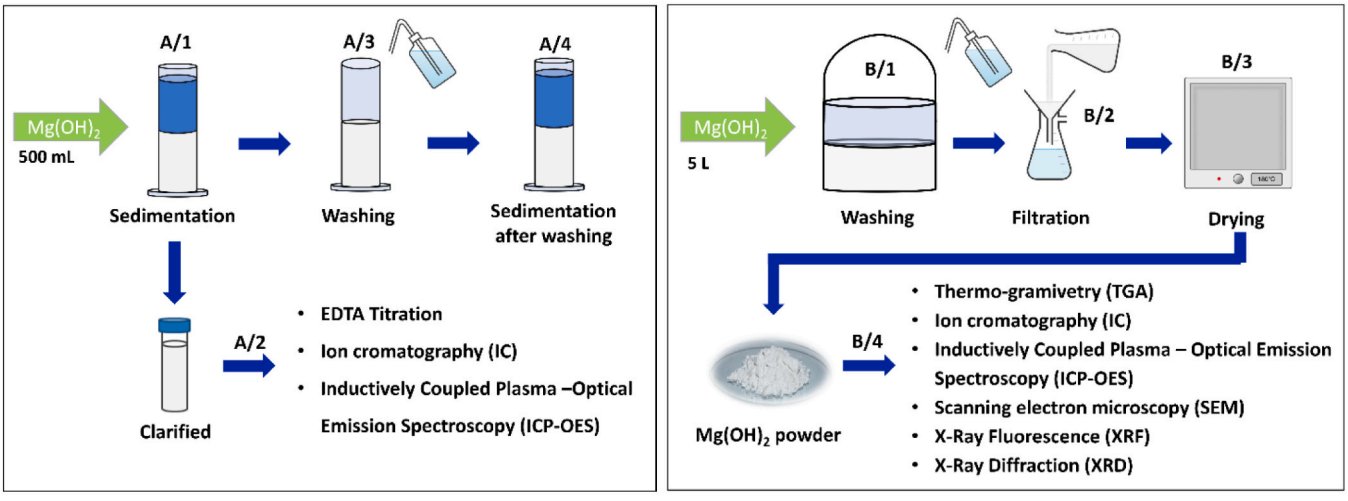

(a) (b)

Fig. 3. Post-treatment procedure of 500 mL (a) and 5 L (b) of $Mg(OH)_2$ suspensions.

$$Cation\ purity = \frac{C_{Mg^{2+}}}{\sum_{i=1}^{N} C_i} \quad (7)$$

where C_i [ppm] is the concentration of *i*-th detected cation, e.g. magnesium, sodium or calcium.

The content of boron was detected by Coupled Plasma Optical Emission Spectrometry (ICP-OES) analysis. 100 mg of dried powders were dissolved in 50 mL of nitric acid solution (Chem-lab; 70 %; HNO_3 ultrapure) and then, analysed using the PerkinElmer Optima 2100 DV spectrometer.

The presence of heavy elements in the powders was assessed through X-ray fluorescence spectroscopy (XRF) analysis. XRF spectra were obtained by Tracer III SD Bruker A.X.S. portable spectrometer (Bruker, U. K.) equipped with a Rhodium Target X-ray tube operating at 40 kV and 11 mA.

The morphology of the powders was also investigated by using the Scanning Electron Microscope FEI Quanta 200 FEG. A gold coating of the powders was adopted to make them conductive. The crystalline structure in the powders was assessed by X-ray diffraction, XRD, RIGAKU model D.MAX 2500 HK, technique in the 2θ range of 10–70° at a step size of 1°/min (CuKa radiation, 40 KV, 40 mA, 1.542° A).

2.5. Techno-economic analysis

A techno-economic analysis was carried out to evaluate the economic feasibility of recovering $Mg(OH)_2$ compounds from SWRO brines by adopting the MF-PFR crystallizer and a inorganic carbon removal pre-treatment step for $Mg(OH)_2$ solids purity enhancement. In the calculation, the typical retentate amount of a RO plant of a small island, as that of Lampedusa, was taken into account, i.e. 4500 m^3/day. The NaOH solution (0.5 M) flow rate was determined by pilot results. In the analysis, the crystallizer section was made of the crystallizer (the MF-PFR), its pumps, a settler and a drum filter, while the inorganic carbon (in the form of CO_2, after brine acidification) removal unit was a stripping column with its packing and a compressor for vacuum.

2.5.1. Capital costs

The purchased cost for base conditions for each piece of equipment, $c^0_{p,Equipment}$, (€), was determined as:

$$log_{10}\left(c^0_{p,Equipment}\right) = K_1 + K_2 \cdot log_{10}(Equip._{Charact.}) + K_3 \cdot \left(log_{10}(Equip._{Charact.})\right)^2 \quad (8)$$

where K_1, K_2 and K_3 are constants that depend on the specific equipment, while $Equip._{Charact.}$ is a characteristic of the equipment, e.g. the volume, see Table 3 for each equipment details.

The bare module cost, $c_{BM,Equipment}$, (€), for each piece of equipment was then calculated:

$$c_{BM,Equipment} = \frac{c^0_{p,Equipment} \cdot CEPCI_{actual}}{CEPCI_{Reference}} \cdot F_{BM,Equipment} \quad (9)$$

where the $CEPCI_{actual}$ and $CEPCI_{Reference}$ are the Chemical Engineering Plant Cost Index from the 2001 and 2023, i.e. 394.3 and 808.8, respectively [17,34].

The total module capital cost, $c_{TM,Equipment}$, (€), is:

$$c_{TM,All\ Equipment} = \sum_i^N c_{BM,i}\left(1 + \alpha_{cont} + \alpha_{fee}\right) \quad (10)$$

where *i* is the i-th piece of equipment, *N* is the total number of pieces of equipment, while α_{cont} and α_{fee} are the multiplication cost factors for contingencies and fees, i.e. 15 % and 5 %, respectively.

2.5.2. Operating costs

The operating costs of the column and the crystallizer, $c_{elec,Crystallizer\ or\ Column}$, (€/y),were evaluated as:

$$c_{elec,Crystallizer\ or\ Column} = cost_{electricity} \cdot Power_{TOT,equipment} \cdot N_{oper,hours} \quad (11)$$

where $cost_{electricity}$, $Power_{TOT,equipment}$ and $N_{oper,hours}$ are the cost of the electricity (€/kWh), the total power of the unit (kW) and the total operating hours of the plant, i.e. 8000 h. The electricity cost was 0.15 €/kWh [35]. The energy consumption of 1.14 kWh/kg-$Mg(OH)_2$ was calculated for the pilot, 0.4 kWh/kg-$Mg(OH)_2$ for filtration and 0.75 kWh/kg-$Mg(OH)_2$ for drying (cake humidity of ~70 %), respectively. The required power for the stripping unit was 0.57 kWh/kg-$Mg(OH)_2$. The cost required for NaOH solution, c_{NaOH}, (€/y),was calculated as:

$$c_{NaOH} = cost_{NaOH} \cdot Q_{NaOH} \cdot N_{oper,hours} \quad (12)$$

where $cost_{NaOH}$ and Q_{NaOH} are the cost of NaOH solution and its flow rate. The cost of NaOH was 330 €/ton [17], assuming it is produced in-situ by an EDBM unit, which also provides the acidic solution required for the brine acidification step for CO_2 stripping (the specific cost of NaOH cover all operating costs, including acid generation). It should be noted, however, that despite the convenient cost for NaOH production by using the EDBM, the option of selling NaOH may be considered and viable if the utilisation site coincides with the plant operational site (e.g. within the desalination plant itself). However, when long-distance transportation is required, the cost of concentration has to be considered (to avoid transporting huge volumes of dilute solutions), which risks to affect the economic viability of this idea.

2.5.3. Net present value (NPV)

The Net Present Value (NPV), (€), was:

$$NPV = -c_{TM,All\ Equipment} + \sum_t^T \frac{R_t - OPEX_t}{(1+i)^t} \quad (13)$$

where *T* is the plant lifetime (here 20 years) and *i* is the discount rate (6 %). R_t is the revenue calculated as the $Mg(OH)_2$ yearly production for its selling price, while $OPEX_t$, are the sum of yearly operating costs for NaOH purchase, i.e. $cost_{NaOH}$, and electricity consumption, $c_{elec,Equipment}$.

Table 3
Constants adopted for the calculation of base purchased costs for each piece of equipment. F_{BM} is the bare module factor of each equipment. Values are taken by [33].

Quantities	K_1	K_2	K_3	$Equip._{Charact.}$ [a]	F_{BM}
MF-PFR crystallizer	4.5097	0.1731	0.1344	Volume, m^3	1.6
Settler	4.8059	−0.3973	0.1445	Volume, m^3	1
Pump	3.3892	0.0536	0.1538	Shaft power, kW	4.92
Drum filter	4.8123	0.2858	0.0420	Filtration area, m^2	1.65
Stripping column	3.4974	0.4485	0.1074	Volume, m^3	9
Packing	2.4493	0.9744	0.0055	Volume, m^3	7
Compressor for vacuum	2.2897	1.3604	−0.1027	Fluid power, kW	2.8

[a] $Equip._{Charact.}$ values were estimated based on the pilot scale plant.

3. Results

In the following section results of the experimental campaign are discussed. Worth noting that the stability of the reactor over time was also assessed through a long-run experiment, whose results are reported in the Appendix A.1.

3.1. Influence of bicarbonate content in the brine, Tests C

Tests C investigated the influence of bicarbonates content in the brine on the features of produced $Mg(OH)_2$ suspensions and solids. In all

cases, the pH was ~10.5 and the Mg^{2+} recovery was ~90 %. Fig. 4a and b shows settling trends and corresponding initial settling velocities of $Mg(OH)_2$ suspensions before and after the washing step, while Fig. 4c shows filtration rate and cake permeability values.

As shown in Fig. 4, the removal of bicarbonate species from the brine did not affect the settling process of synthesized suspensions. Suspensions produced in tests C1 and C2 exhibited similar initial settling velocity values of 339 ± 20 mm/h and 327 ± 20 mm/h. These values are two times faster than the highest settling rate reported by Turek and Gnot [19], thanks to the controlled precipitation conditions achieved in the MF-PFR prototype. Interestingly, the washing step considerably enhanced the settling velocity, which increased from 339 ± 20 mm/h and 327 ± 20 mm/h to 556 ± 20 mm/h and 612 ± 20 mm/h in tests C1 and C2, respectively.

The improvement of settling features was attributed to the lower electrostatic interactions between particles occurring in the suspension. Note that, the higher the ionic strength of a solution the higher the interactions between particles [36]. In fact, electrostatic interactions can lead to surrounding liquid to be entrapped among particles, forming structures with small specific gravity and therefore low sedimentation rates. On this basis, the washing step is expected to reduce interaction between particles, lower ionic strength of the suspension, thus favouring settling performances of the suspensions.

Suspensions produced in test C1 and C2 had close filtration rate and permeability values, namely 4.9 ± 0.5 kg/m^2 h and 4.0 ± 0.5 kg/m^2 h, and 4.3 ± 0.4 E-6 m^2/bar min and 3.6 ± 0.4 E-6 m^2/bar min, respectively. Filtration rates are in line with data reported by Turek and Gnot [20], notwithstanding the faster initial settling rate. Cake permeability values are also in accordance with data reported by Morgante et al. [22] and Roa et al. [37] for synthetic and real Mg^{2+}-containing solutions with a Mg^{2+} concentration of ~5.8 g/L and 1.6 g/L, respectively. It should be noted that, the comparison between initial settling velocities should also take the magma density of the suspensions into account. On the other hand, these data are not always available. For the sake of completeness, Table A2 reports the magma densities of $Mg(OH)_2$ suspensions produced in the present work.

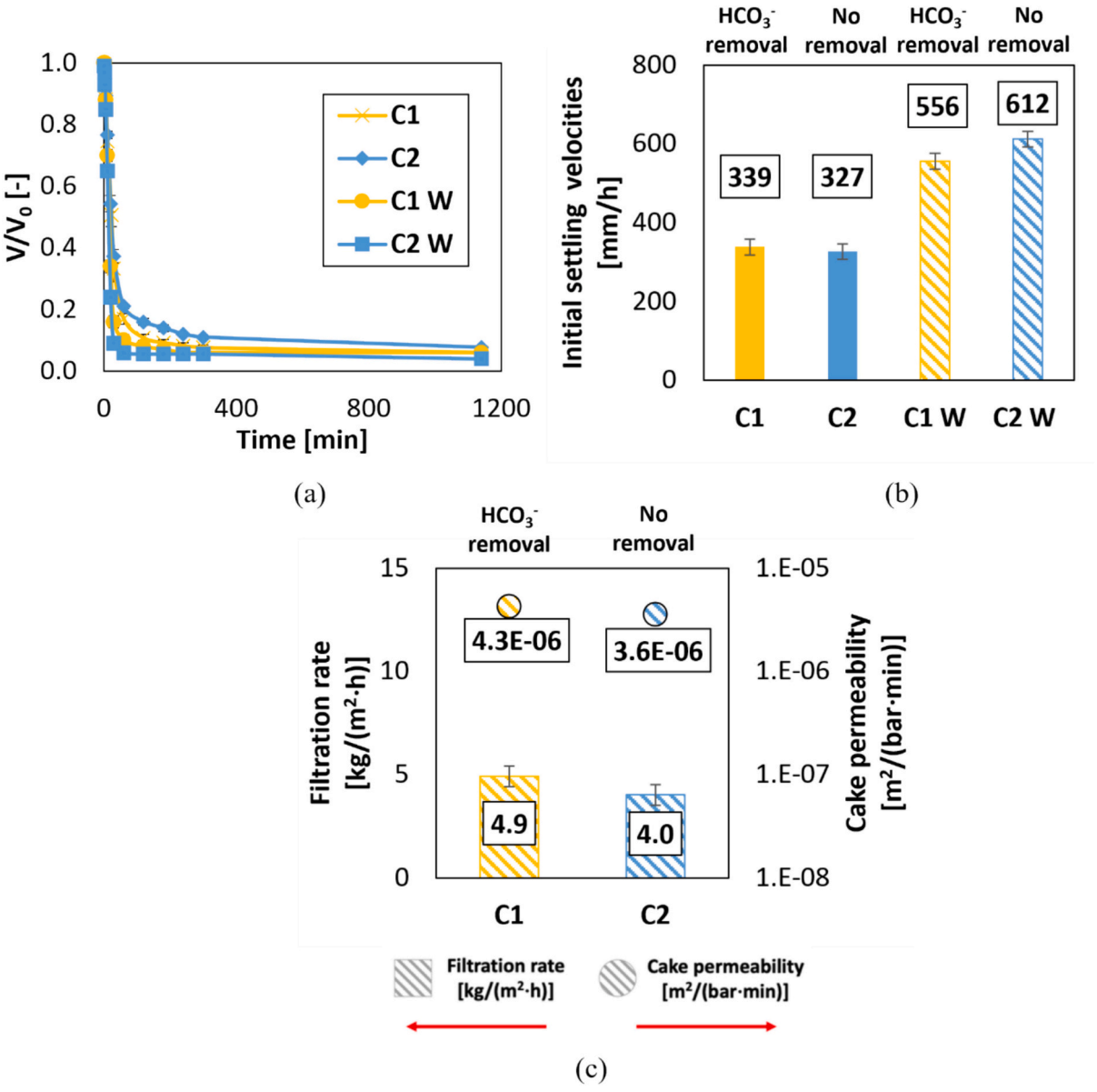

Fig. 4. Tests C: (a) settling trends and (b) initial settling velocities of $Mg(OH)_2$ suspensions collected in tests C1 and C2 before and after the washing step; (c) filtration rates (bars) and cake permeability (circle symbols) values. The letter W refers to washed samples. V is the instantaneous volume of settling suspensions, while V_0 is the initial one, i.e. 500 mL.

The cationic and mass purity of synthesized $Mg(OH)_2$ solids, evaluated by Eqs. (7) and (A.1), are shown in Fig. 5.

As can be seen in Fig. 5, the bicarbonate removal step was essential to synthesize higher purity $Mg(OH)_2$ solids. Cationic purity was higher than 98.3 % in samples produced in test C1, while the purity decreased to 93.8 % in samples synthesized in tests C2, due to the presence of Ca^{2+} (Ca^{2+} content was 5 %, ~18.54 $\frac{mg}{g_{Mg(OH)_2}}$, in samples C2, while it was lower than its limit of quantification (LOQ) of ~1.3 $\frac{mg}{g_{Mg(OH)_2}}$ in samples C1). In all solids, the concentration of sodium (Na) ions was always lower than its limit of quantification of 5 $\frac{mg}{g_{Mg(OH)_2}}$ (LOQ). This behaviour agrees with data reported by Vassallo et al. [27] after their bicarbonate removal step. TG analyses indicated a mass purity of ~97.8 % of $Mg(OH)_2$ solids precipitated in tests C1, while the purity was 94 % in samples C2. In this latter case, TG analysis reported a Ca^{2+} content of ~20.06 $\frac{mg}{g_{Mg(OH)_2}}$, in accordance with IC analysis, which precipitated in the form of calcium carbonate (see Fig. A3).

A widely used approach to recover Mg^{2+} and Ca^{2+} from seawater brines includes a separation of monovalent and bivalent ions through NF technology. In this regards, similar Mg^{2+} recoveries (~90 %) and Mg $(OH)_2$ solids purity (~94 %, due to the coprecipitation of Ca^{2+}) could be noted by comparing results of the C2 test (without CO_2-stripping pretreatment) and those reported by Morgante et al. [23]. The latter related to the production of $Mg(OH)_2$ at a pH value of 10.6 using NaOH solutions treating a retentate stream of a nanofiltration (NF) unit fed by SWRO brines, Mg^{2+} and Ca^{2+} concentrations of 4.6 g/L and 1.4 g/L, respectively. This can be attributed to the similar Mg^{2+} and Ca^{2+} ratio in the two solutions, i.e. 2.9 and 3.3 for SWRO and NF retentate brines, respectively.

3.2. Influence of the alkaline solution flow rate, Tests N

Tests N were carried out by varying the flow rate of the alkaline solution. In all tests, the brine was pre-treated to reduce the amount of bicarbonates. Reaction pH values, magnesium, and calcium recoveries, Eq. (2), are shown in Fig. 6.

The pH of the produced $Mg(OH)_2$ suspensions increased from 10 up to 12.4, varying the alkaline flow rate from 24 L/h to 47 L/h, as shown in Fig. 6.a. The magnesium recovery increased from ~65 %, at the pH value of 10, to ~100 % already at a pH value of 11.2. The calcium recovery was almost null up to a pH value of 11.2, while it increased at higher values, Fig. 6.b, probably due to the precipitation of residual bicarbonates in the brine.

Fig. 7 reports settling trends, initial settling velocities, filtration rates and cake permeability values observed by increasing the NaOH flow rate.

Suspensions exhibited faster settling and filtration characteristics increasing the alkaline solution flow rate up to the value of 38 L/h (test N4) reaching initial settling velocity, filtration rate and cake permeability values of 417 ± 20 mm/h, 6.5 ± 0.5 kg/m^2h and 5.7 ± 0.4 E-06 m^2/bar min, respectively. A further increase of the alkaline flow rate caused a strong reduction of these features, reaching values of ~39 ± 10 mm/h, 1.9 ± 0.3 kg/m^2h and 1.6 ± 0.4 E-06 m^2/bar, respectively, in test N6. This behaviour can be explained considering the (i) the Zeta-potential of $Mg(OH)_2$ particles, (ii) the lyosorption phenomenon and (iii) the local supersaturation in the reaction environment. The Zeta-potential of $Mg(OH)_2$ particles has been reported to vary from +25 mV to −25 mV at pH values from 10 to 13, being null at a pH of ~12 [38]. The lyosorption phenomenon leads to the formation of lyospheres, which are agglomerated particles that entrap surrounding liquid, with low gravity density. This phenomenon is favoured at high pH values [20]. The local supersaturation affects crystallization phenomena. In particular, the higher the supersaturation the higher the nucleation phenomena. Nucleation leads to tiny particles with low settling and filtration features [38]. Therefore, on the one hand, the increase of the pH, from tests N1 to N4, caused a reduction of the Zeta-potential value of the particles, thus promoting the aggregation phenomena, leading to big particles characterized by fast settling and filtration characteristics. On the other hand, the higher the pH the higher the influence of the lyosorption and nucleation phenomena that hindered the settling and filtration processes in tests N5 and N6. As far as the purity of synthesized powders is concerned, cationic and mass purities were >98.3 % and ~98 % in samples precipitated up to pH values of 11.2, while they were ~97.8 % and 97 % in samples produced at pH values higher than 12. This was attributed to the co-precipitation of calcium compounds. Note that, the washing step again favoured the settling process, though the relevant trends are here omited for the sake of brevity.

3.3. Influence of the brine flow rate, Tests F

Tests F were carried out by increasing the flowrate of the brine solution from 50 L/h to 150 L/h. In all tests, the suspension pH was 10.5 and a Mg^{2+} conversion of 90 % was achieved. The flow rate of the alkaline solution was varied to keep the pH value of the outlet suspension constant. Fig. 8 shows settling trends, initial settling velocities, filtration rates and cake permeability values for tests F.

The increase of brine flow rate hindered the settling and filtration properties of $Mg(OH)_2$ suspensions. The initial settling velocity decreased from ~405 ± 20 mm/h to ~112 ± 15 mm/h, increasing the brine flow rate from 50 L/h to 150 L/h,(see Fig. 8.b), while filtration rates and cake permeability values varied from 7.2 ± 0.5 kg/m^2 h and 6.3 ± 0.4 E-6 m^2/bar min to 2.2 ± 0.3 kg/m^2 h and 1.9 ± 0.4 E-6 m^2/

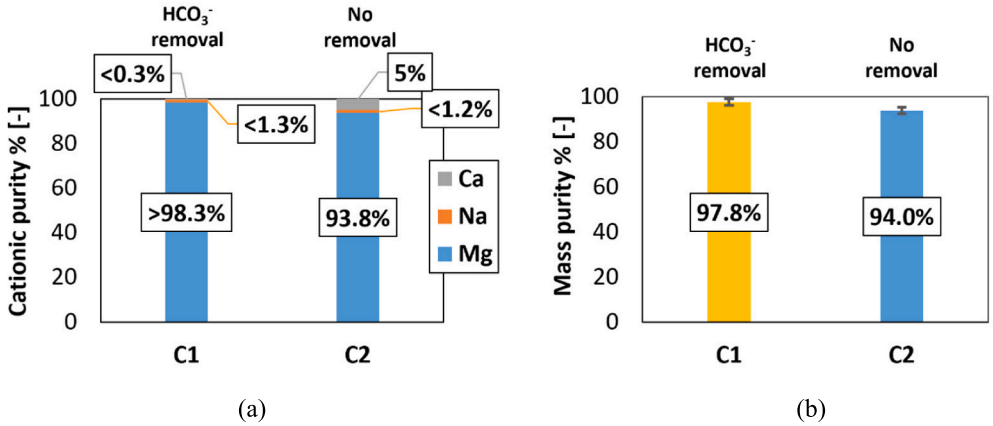

Fig. 5. Cationic purity (a) and mass purity (b) values of $Mg(OH)_2$ solids synthesized in Tests C. Na^+ and Ca^{2+}limit of quantifications (LOQ), in IC analysis, were 5 and 1.3 $\frac{mg}{g_{Mg(OH)_2}}$, respectively.

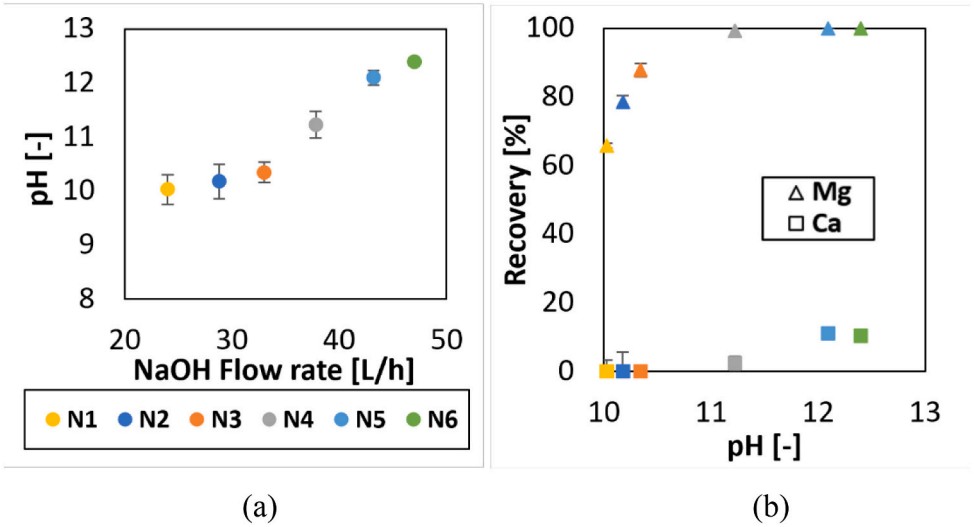

Fig. 6. Tests N: (a) pH values of $Mg(OH)_2$ suspensions as a function of NaOH solution flow rates; (b) magnesium and calcium recovery, achieved at different pH values.

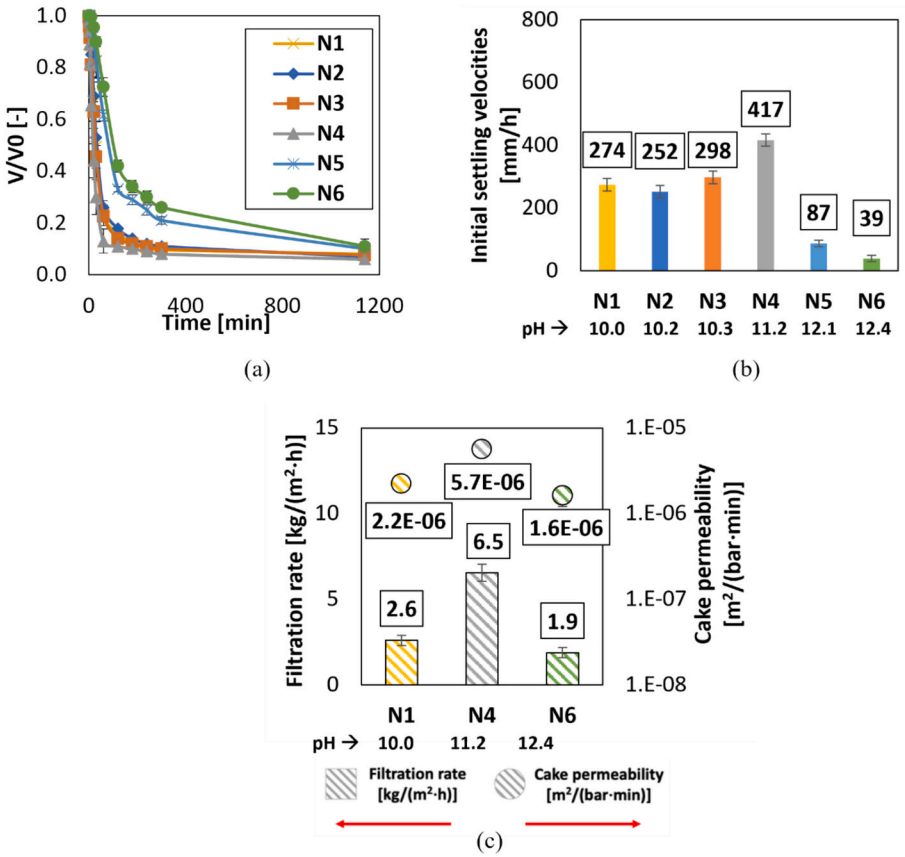

Fig. 7. Tests N: (a) settling trends; (b) initial settling velocities; (c) filtration rates (bars) and cake permeability (circle symbols) values obtained by increasing the pH value of the suspension from 10 to 12.4. V is the instantaneous volume of settling suspensions, while V_0 is the initial one, i.e. 500 mL.

bar min, respectively. This behaviour was attributed to (i) the lower residence time of $Mg(OH)_2$ particles in the reactor and (ii) different fluid dynamic regime inside the reactor. Short residence times reduce particles cementation phenomena, due to less collision probability, forming smaller aggregates with scarse settling and filtration characteristics. In addition, high brine flow rates increase local mixing degree in the reactor due to stronger injection streams that enhance local shear stresses, leading to the formation of small particles with worse thickening and filtration characteristics [38]. In all cases, the cationic purity of $Mg(OH)_2$ powders was higher than 98.5 %, while mass purity was ~98 %.

3.4. Concentration of micro and macro elements in $Mg(OH)_2$ powders

The concentration of micro and macro elements in $Mg(OH)_2$ powders must comply with market requirements for powders applicability. Fig. 9

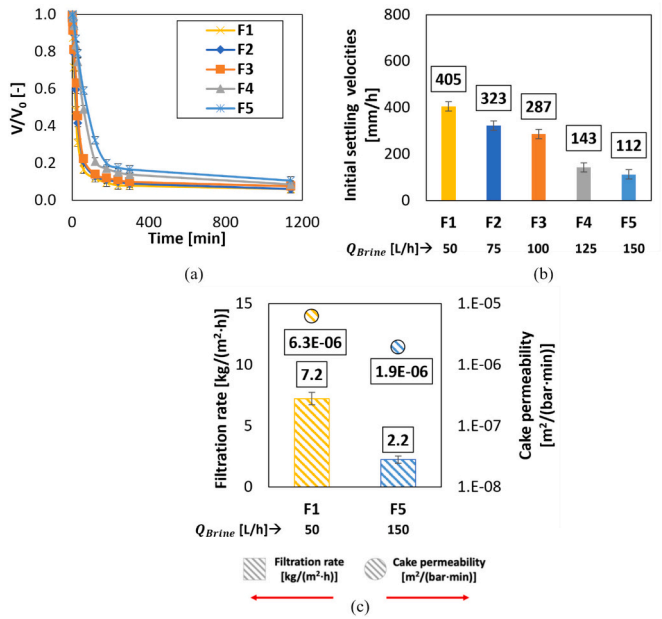

Fig. 8. Tests F: (a) settling trends; (b) initial settling velocities; (c) filtration rates and cake permeabilities values. V is the instantaneous volume of settling suspension, while V_0 is the initial one, i.e. 500 mL.

shows the boron content in synthesized $Mg(OH)_2$ solids and clarified solutions assessed by ICP analysis in Tests N. Boron concentration in clarified solutions of tests N1 and N4 were lower than the Limit of Quantification, but higher than the Limit of Detection. Values of the boron concentrations of clarified solutions of samples N1, N4 and N6 take the dilution process in the reactor due to the mixing of the brine and the NaOH solutions into account.

The increase of the flow rate of the alkaline solution from 24 L/h (test N1) to 47 L/h (Test N6) reduced the boron content from 0.70 $\frac{mg}{g_{Mg(OH)_2}}$ to 0.19 $\frac{mg}{g_{Mg(OH)_2}}$ in the $Mg(OH)_2$ powders. Consequently, the boron content in the clarified solution reached a value as that in the virgin brine. This behaviour is due to the lower boron adsorption on $Mg(OH)_2$ particles at high pH values [39,40]. It is worth noting that, a pre-treatment of the brine would be necessary if $Mg(OH)_2$ powders were to be adopted in the refractory industry.

Fig. 10 shows the XRF spectra of $Mg(OH)_2$ solids produced in tests C1 and C2. Spectra were compared to the one obtained by Magnifin® H10, a commercial $Mg(OH)_2$ solid (used as a flame retardant) characterized by a purity higher than 99.8 % [41].

As it can be observed, the concentration of heavy compounds was comparable to that of the commercial reference Magnifin® solids, thus indicating a high purity of the synthesized powders from seawater brines. It is worth observing that the removal step of bicarbonate species was crucial to reduce the calcium amount in the powders. As a matter of fact, samples C2 showed the presence of Ca, while, sample C1, after the bicarbonate removal, followed the same trend of the Magnifin H10.

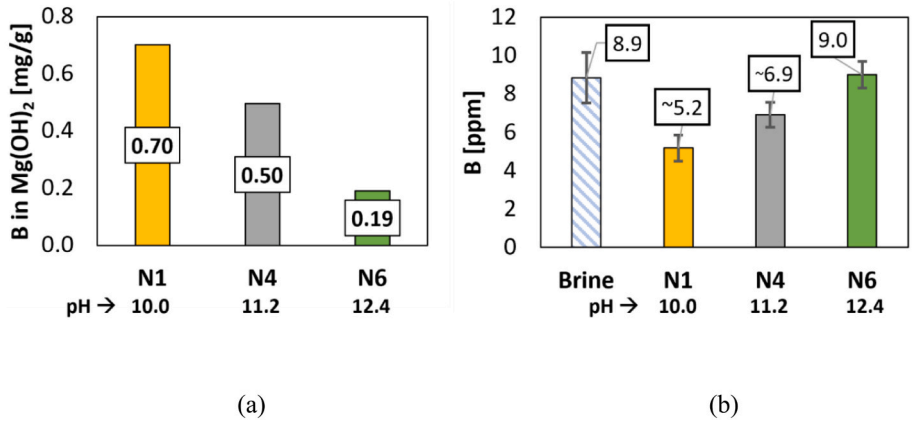

Fig. 9. Boron content in magnesium hydroxide samples (a) and clarified solutions (b) produced in tests N1, N4 and N6.

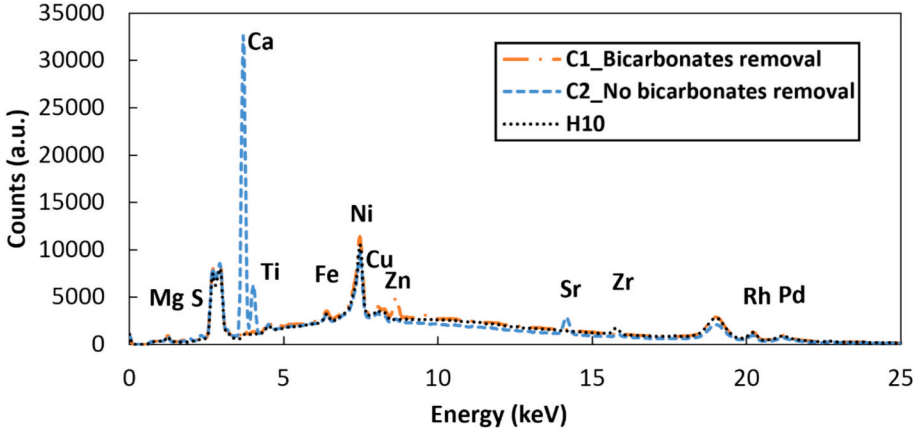

Fig. 10. XRF spectra of $Mg(OH)_2$ solids synthesized in tests C1 and C2. For the sake of comparison, spectra of the commercial Magnifin H10 powders are reported.

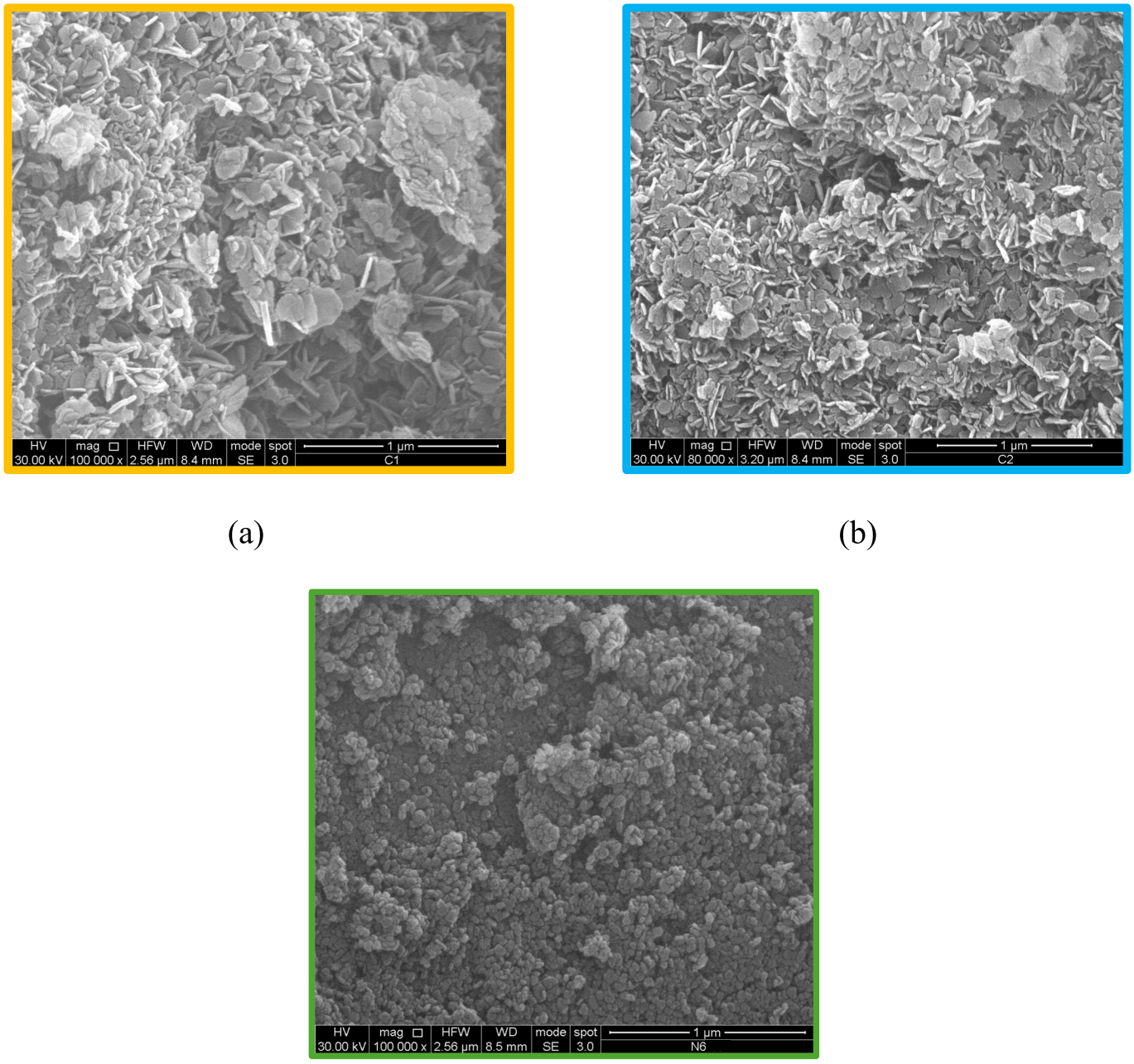

Fig. 11. SEM images at a magnification of 100,000× of $Mg(OH)_2$ solids produced in tests: (a) C1/N3, (b) test C2 and (c) test N6.

3.5. Morphology and crystalline structure of the produced magnesium hydroxide solids

The influence of the brine pre-treatment and the final pH value of $Mg(OH)_2$ slurries on particle morphology was assessed by observing SEM images of $Mg(OH)_2$ solids synthesized in tests C1 (similar condition of test N3), C2 and N6 (Fig. 11).

Interestingly, $Mg(OH)_2$ hydroxide solids produced in tests C1 (or N3) and C2 were aggregate nanoparticles with a hexagonal plate-like shape. In the literature, plate-like crystals were reported by Dong et al. [21] adopting NH_4OH reagents, while, in most of the cases, nanometric globular particles were reported when adopting NaOH solutions [42]. The plate-like shape was attributed to the low supersaturation level attained in the reactor volume due to (i) the low Mg^{2+} content in the brine and (ii) the particular reactor configuration of the MF-PFR. Notwithstanding the hexagonal plate-like shape of the particles, bigger crystals would be necessary for their use as flame retardant fillers. Particles do not differ much between tests C1 and C2, thus suggesting a negligible influence of the co-precipitation of calcium compounds in samples C2. On the other hand, the morphology of $Mg(OH)_2$ particles considerably varied in Tests N6. In this case, aggregated globular shaped nanoparticles forming cauliflower structures can be observed. This was attributed to the higher reaction pH value (12.4) attained in tests N6 that affected the supersaturation level of the system promoting nucleation

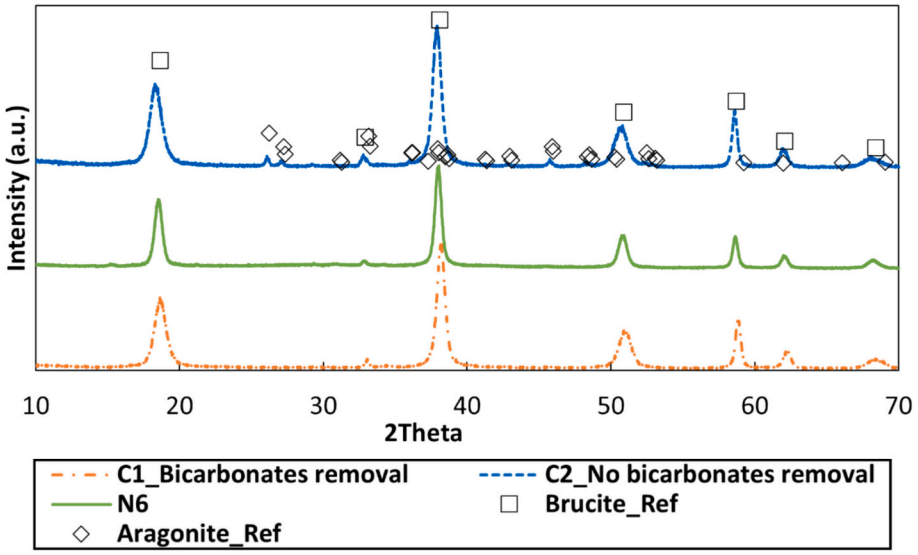

Fig. 12. XRD spectra of $Mg(OH)_2$ solids produced in tests: C1, C2 and N6. Reference spectra of $Mg(OH)_2$ and $CaCO_3$ (aragonite) species were taken from RRUFF™ database [43].

Table 4
A comparison between, Mg^{2+} recovery, $Mg(OH)_2$ purity, settling rate, cake permeability, θ_{perm}, filtration rate and morphology of $Mg(OH)_2$ solids synthesized in several literature studies treating seawater brines. Between brackets the adopted alkaline solution.

	Feed brine (Mg^{2+} conc.)	Investigation scale (brine volume)	pH	Magma density [g/L]	Mg^{2+} Recovery %	Mass Purity [%]	Settling rate [mm/h]	θ_{perm} [m^2/min·bar]	Filtration rate [kg/m^2 h]	Morphology
Present work (NaOH)	Seawater brine (2.4 g/L)	Pilot scale (50–150 L/h)	10–12.4	2.5–3.2	67–100	94–98.5	39–417	1.6–6.0 E-6	1.9–7.2	Platelet like (pH 10.4), Cauliflower (pH 12.4)
Battaglia et al. [24] (NaOH)	Saltwork bittern (49 g/L)	Pilot scale (12–30 L/h)	10.8–12.8	10–25	93–100	98–99.6	–	0.2–6.8 E-6	–	Globular
Morgante et al. [22] (NaOH)	Synthetic brine (5.8–24.3 g/L)	Pilot scale (40–120 L/h)	10–12	5–10	65–100	–	–	0.4–1.4 E-6	–	–
Turek and Gnot [20] (NaOH)	Coal mine brine (2.84 g/L)	Lab scale (350 mL)	–	~4	61.2	–	72–170	–	3–9.1	–
Dong et al. [21] (NH_4OH)	Seawater brine (1.68 g/L)	Lab scale (200 mL)	10–10.2	~4	20–90	93.5	–	–	–	Platelet-like
Dong et al. [42] (NaOH)	Seawater brine (1.72 g/L)	Lab scale (200 mL)	11.2–13.4	~4	94–99	89–94	–	–	–	Globular

Table 5
CAPEX, OPEX for reagents, OPEX for electricity consumption and NPV values to produce $Mg(OH)_2$ from SWRO brine in the three investigated scenarios.

	CAPEX [Million €]	OPEX for reagents [Million €/y]	OPEX for electricity [Million €/y]	NPV [Million €]
Case #1	2.17	3.26	2.23	9.3
Case #2	3.37	3.26	2.79	1.5
Case #3	3.37	3.26	2.79	16.7

phenomena.

Fig. 12 shows the XRD spectra of $Mg(OH)_2$ solids.

Brucite, namely $Mg(OH)_2$, was the main phase in all samples. Traces of aragonite, i.e. calcium carbonate, were observed only in powders produced in test C2, confirming the effectiveness of the inorganic carbon removal step.

3.6. Comparison among performance parameters of different $Mg(OH)_2$ precipitation studies

For the sake of completeness, Table 4 reports a summary of performance parameters obtained in different $Mg(OH)_2$ precipitation studies. Seawater brines were mainly studied at a laboratory scale (Mg volume of ~hundreds of mL), while real and synthetic more concentrated Mg^{2+}-containing solutions were analysed at a pilot scale (Mg flow rates of ~tens or hundreds of L/h). Magma densities (before settling) ranged between 2.5 and 4 g/L when studying seawater brines, while values were up to 25 g/L treating saltworks bitterns. Mg^{2+} recovery reached values up to ~100 % by using NaOH solutions as the alkaline reactant, while the highest recovery of ~90 % was achieved by adopting NH_4OH. Powder purity was about 99.6 % in $Mg(OH)_2$ solids produced from saltworks bitterns, thanks to the low Ca^{2+} concentration in these solutions, while purity was ~94 % from seawater brines. The value of 98.5 %

was here achieved thanks to the CO_2 removal from the solution. In the present work, settling rates were up to 417 mm/h against the highest value of 170 mm/h reported in the literature (suspensions with similar magma density). Filtration characteristics (θ_{perm} and filtration rate) are overall close to each other in research. Platelet-like crystals were reported when adopting NH_4OH solutions, while globular particles were mainly observed employing NaOH ones. Interestingly, in the present work, the use of the novel MF-PFR prototype allowed both morphologies to be obtained by controlling the pH environment.

3.7. Techno-economics scenarios

Three scenarios were studied: (i) no pretreatment of the brine (no column) and price of $Mg(OH)_2$ of 1000 (€/ton, [17]), Case #1; (ii) pretreatment of the brine and price of $Mg(OH)_2$ of 1000 (€/ton), Case #2; (ii) pretreatment of the brine and price of $Mg(OH)_2$ of 1200 (€/ton [18]) thanks to the higher purity, Case #3. CAPEX, OPEX and NPV values are reported in Table 5.

The use of the pre-treatment was found to considerably account both CAPEX and OPEX of the process, being values ~55 % and ~20 % higher than those of the case without the pre-treatment step. On the other hand, the higher purity is expected to increase the price of the produced Mg $(OH)_2$ solids, thus allowing the NPV to almost double with respect to the no pre-treatment case. In all scenarios, the process was found to be profitable. Purity, morphology, size, and degree of aggregation among particles can significantly affect the commercial value of $Mg(OH)_2$ particles, therefore, thanks to the high purity of here synthesized Mg $(OH)_2$ powders, after post-treatment for morphology adaptation, solids could be sold in flame retardant application at a price up to 2000 €/ton, thus making the recovery of $Mg(OH)_2$ from brines even more profitable.

It is worth noting that the economic analysis is based on data from literature and pilot scale experience, thus an improvement can be expected considering a specific tailored design for a specific plant. In addition, the circularity of the Brine To Value project was not taken into account. In this latter case, all the chain would have benefits from the recovery of $Mg(OH)_2$ and further economic benefits should be considered (the re-use of the CO_2 and the mix of Ca^{2+} and Mg^{2+} species in loco to remineralize the permeate stream, thus not requiring the purchase of chemicals in the RO plant).

4. Conclusions

The present work assessed the $Mg(OH)_2$ production at a semi-industrial scale by integrating a pilot scale crystallizer into a real RO desalination plant. Activities were carried out on the island of Lampedusa, Sicily (Italy). Real seawater brines were fed to the reactor, and NaOH solutions adopted as alkaline reagent. A purposely designed prototype crystallizer, namely the Multi Feed Plug Flow Reactor, MF-PFR, was employed to treat the RO brine. The influence of (i) brine pre-treatment to remove bicarbonates (acidification of the brine and stripping), (ii) pH reaction and (iii) brine flow rate was assessed on the (i) settling and filtration rates of produced $Mg(OH)_2$ suspensions, (ii) purity of $Mg(OH)_2$ powders, (iii) content of micro and macro elements in $Mg(OH)_2$ powders, and (iv) morphology of the solids.

The pre-treatment of the brine was a fundamental step in synthesizing highly pure $Mg(OH)_2$ solids. In fact, mass and cationic purity increased from ~94 % to ~98 % thanks to the pre-treatment, which did not affect the settling and filtration characteristics of synthesized suspensions, as well as the morphology of the particles. On the other side, bicarbonates removal resulted in the recovery of CO_2 useful for the remineralisation of the permeate in the wider process scheme of the Brine to Value project, boosting the development of sustainable solutions for circular desalination.

The reaction pH was found to be also a crucial parameter. The higher the pH, the higher the Mg^{2+} conversion, being almost 100 % already at pH 11.2. At this pH condition, the highest settling and filtration rates were obtained, with initial settling velocity, filtration rate and cake permeability values of 417 ± 20 mm/h, 6.5 ± 0.5 kg/m^{2}h and 5.7 ± 0.4 E-06 m^2/bar min, respectively. Note that, the settling rate was 2.5 times faster than the highest velocity reported in the literature, thanks to the innovative design of the reactor and the optimized operating conditions. pH values higher than 12 caused a strong reduction of the initial settling velocity, filtration rate and cake permeability. This was attributed to the influence of (i) Zeta-potential of $Mg(OH)_2$ particles, (ii) lyosorption phenomenon and (iii) local supersaturation in the reaction environment attained at different operating conditions. On the other hand, the higher the pH the lower the boron content in the $Mg(OH)_2$ solids. To comply with the refractory industry, however, a pre-treatment of the brine must be performed to reach the market boron concentration target. The pH also affected the morphology of the powders that were nanoparticles with a hexagonal plate-like shape at a pH value of 10.5, while nanometric globular particles were observed at a pH value of 12. Hexagonal platelets are rarely reported in the literature when adopting NaOH solutions, suggesting here a good control of the supersaturation level inside the reaction environment. However, the presence of nanosized particles makes them still not yet suitable for flame retardant applications. In all tests, the concentration of macro elements in the powder was found to be negligible, marking the high purity of the $Mg(OH)_2$ solids.

The influence of the hydrodynamics of the reactor, specifically the flow rate of the brine, considerably affected the filtration and settling characteristics of the suspensions. High residence times and low injection energies of the brine stream were found to be the best operating strategy for synthesizing suspensions with high settling and filtration properties. Of course, despite a lower productivity of the plant. A preliminary techno-economics analysis proved the economic feasibility of the process with and without the pre-treatment step of inorganic carbon removal.

Finally, the optimal Mg-recovery target was found to be tuneable and adapted to different possible scenarios, among which, also the case of a double step precipitation aiming at the recovery of a remineralisation mix of Mg and Ca, able to internally address the need for chemicals supply in circular desalination concepts.

In summary, some take home guidelines for the $Mg(OH)_2$ production from saline solutions to be adopted in other locations with different SWRO brines are: (i) pH values higher than 11.2 should be adopted to achieve a Mg^{2+}recovery higher than 99 %; (ii) pH values higher than 12.4 should be used to reduce the boron content in $Mg(OH)_2$ particles; (iii) mass and cation purity values lower than 95 % will be obtained if calcium and inorganic carbon ions are present in the brine, while a reduction of the concentration of one of the two can lead to purities higher than 98.5 %, (iv) settling and filtration rates of $Mg(OH)_2$ suspensions and powder morphology will strongly depend on the adopted operating conditions and chosen reactors.

Nomenclature and abbreviations

CAPEX	Capital Expenditure
EDBM	Electrodialysis with bipolar membranes
EDTA	Complexometric titration with ethylenediaminetetraacetic acid
IC	Ion Chromatography
ICP-OES	Inductively Coupled Plasma Optical Emission Spectroscopy
LOQ	Limit of quantification
MF-PFR	Multi Feed Plug Flow Reactor
NF	Nanofiltration
NPV	Net Present Value
OPEX	OPerational EXpenditure
RO	Reverse Osmosis
SEM	Scanning Electron Microscope
SWRO	Seawater Reverse Osmosis
TG or TGA	Thermogravimetric analysis
XRF	X-ray fluorescence spectroscopy
W	Washed samples
θ_{perm}	Cake permeability coefficient, [m^2/(bar min)]
Q_{Brine}	Feed brine flow rate, [L/h]
Q_{NaOH}	Alkaline flow rate, [L/h]
V	Instantaneous volume of settling suspensions, [mL]
V_0	Initial volume of settling suspensions, [mL]

CRediT authorship contribution statement

Lorenzo Ventimiglia: Methodology, Validation, Formal analysis, Investigation, Data curation, Writing – original draft, Visualization. **Fabrizio Vassallo:** Conceptualization, Methodology, Investigation. **Giuseppe Lo Burgio:** Methodology, Investigation. **Antonino Campione:** Conceptualization, Methodology, Resources, Writing – review & editing, Supervision, Project administration, Funding acquisition. **Laura Cammilli:** Project administration. **Paolo Vicario:** Project administration. **Giuseppe Battaglia:** Methodology, Validation, Formal analysis, Data curation, Writing – original draft, Visualization, Supervision. **Fabrizio Vicari:** Conceptualization, Methodology, Resources, Supervision. **Andrea Cipollina:** Conceptualization, Methodology, Resources, Writing – review & editing, Supervision, Project administration, Funding acquisition. **Alessandro Tamburini:** Conceptualization, Resources, Supervision, Funding acquisition. **Giorgio Micale:** Conceptualization, Resources, Supervision, Funding acquisition.

Declaration of competing interest

The authors declare that they have no known competing financial interests or personal relationships that could have appeared to influence the work reported in this paper.

Acknowledgments

The authors acknowledge the financial support of SUEZ International for the activities of the Brine to Value project.

Appendix A

A.1. Stability of the reactor

A long run test of about 5 h was carried out to investigate the stability and the functioning of the reactor over time. The same operating parameters of test C1 were adopted, see Table 2. Samples were collected at 30, 45, 60, 120, 180 and 240 min after the beginning of the test. Fig. A1 shows settling trends, calcium and magnesium recoveries, Eq. (2), over time.

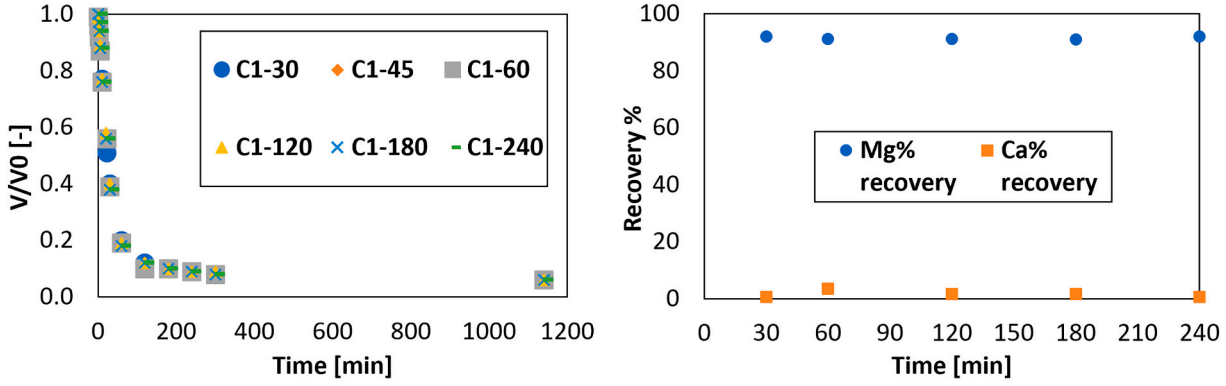

Fig. A1. Stability test: (a) settling trend of suspensions collected at different experimental times; (b) Ca^{2+} and Mg^{2+} recoveries, Eq. (2). V is the instantaneous volume of settling suspension, while V_0 is the initial one, i.e. 500 mL.

$Mg(OH)_2$ suspensions produced over time exhibited the same settling features, see Fig. A1.a. Ca^{2+} and Mg^{2+} recoveries were almost constant over time, Fig. A1.b, thus indicating a very good stability of the system.

A.2. Evaluation of the initial settling velocity

Settling study provided values of instantaneous volume of the settling suspension, $V(t)$, over time. To calculate the initial settling velocity, $V(t)$

values were divided by the cross-sectional area of the adopted graduated cylinder obtaining instantaneous heights, $H(t)$, over time, see Fig. A2.

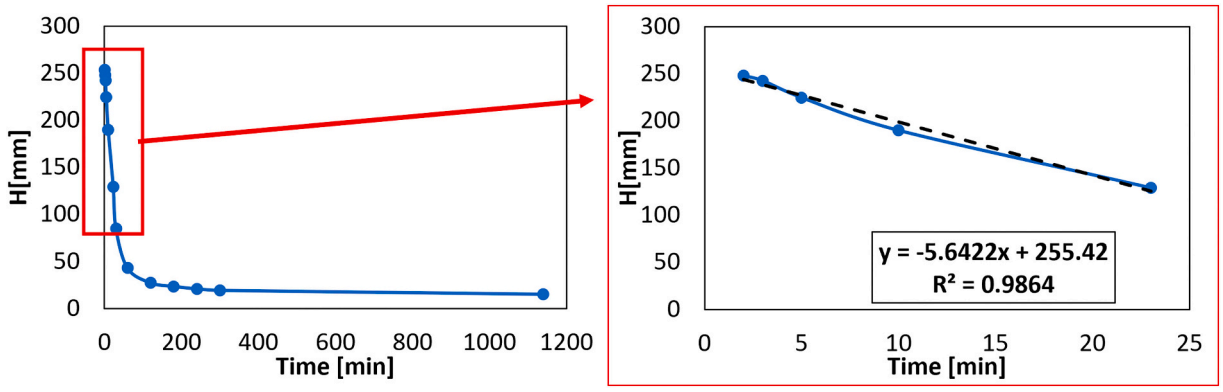

Fig. A2. (a) Instantaneous height points of $Mg(OH)_2$ suspensions during settling in a 500 mL graduated cylinder over time. (b) An insight of the first 30 min. Data were collected in test C1.

The initial settling velocity was the slope of the settling curve evaluated by a linear regression detected from the 2nd to the 20th minute of the process, as highlighted in the Fig. A2b.

A.3. Evaluation of the mass purity of $Mg(OH)_2$ solids

The mass purity of $Mg(OH)_2$ powders was calculated as the ratio between the mass loss detected in the temperature range 320 °C - 800 °C, ($\Delta m_{320-800°C}$), and the theoretical ($\Delta m_{theoretical}$) one, i.e. 30.8 % [44]:

$$Mass\ purity = \frac{\Delta m_{320-800°C}}{\Delta m_{theoretical}} \tag{A.1}$$

In the presence of other compounds, attention must be paid to possible other mass losses in the selected temperature range. In the latter case, the graphical method presented by Dong et al. [42] can be adopted. As an example, Fig. A3 shows the TG and DTG plots of $Mg(OH)_2$ solids synthesized in tests C2 (samples containing also calcium carbonate species).

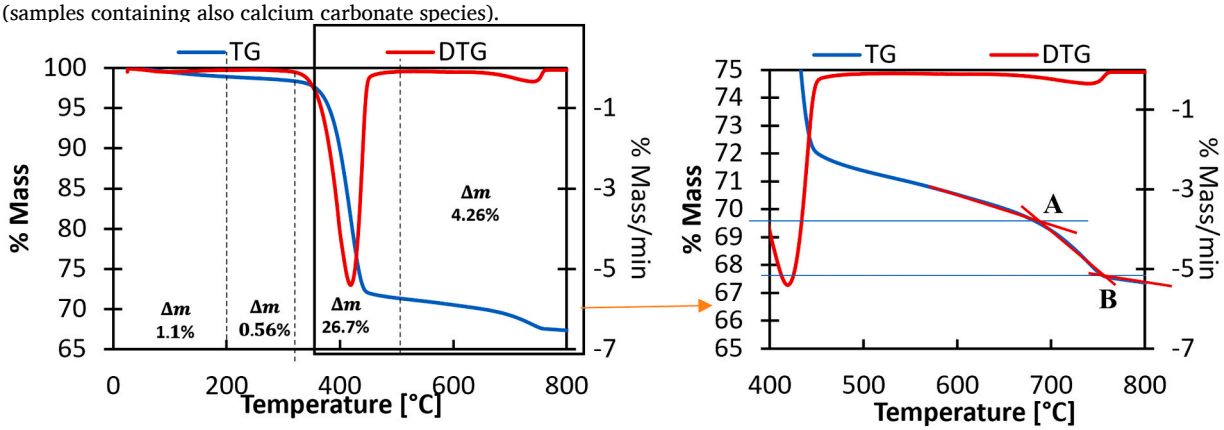

Fig. A3. (a) TG and DTG plots of $Mg(OH)_2$ powders synthesized in test C2. (b) Details of the graphical method adopted for the evaluation of the mass drop due to the presence of $Ca(CO)_3$ species in the powders.

Two main mass losses can be observed: one in the temperature range between 300 and 480 °C, due to the decomposition of $Mg(OH)_2$ into magnesium oxide; a second in the temperature range between 650 °C - 750 °C due to the degradation of calcium carbonate in calcium oxide [42]. The mass loss due to the degradation of $CaCO_3$ was identified by drawing three straight lines tangent to the TG curve, before, during and after the mass change in the 650 °C and 750 °C temperature range, see Fig. A3.b. The calcium content was then calculated by the difference of the mass losses identified by the intersection of the lines as reported in Eq. (A.2):

$$C_{Ca} = \frac{(m_A - m_B)}{100} \cdot \frac{Mw_{Ca}}{Mw_{CO2}} \tag{A.2}$$

where m_A and m_B are the mass value at point A and B in the TG graph, while Mw_{Ca} and Mw_{CO2} are the molecular weights of Ca and CO_2 species.

Eq. (A.1) can be then rewritten as.

$$Mass\ Purity\ of\ Mg(OH)_2 = \frac{\Delta m_{320-800°C} - (m_A - m_B)}{\Delta m_{theoretical}} \tag{A.3}$$

A.4. Cake humidity

For the sake of completeness, the humidity of $Mg(OH)_2$ cakes are reported in Table A1.

Table A1
Humidity content in $Mg(OH)_2$ cakes synthesized in the present work, see Table 2 for further details.

Tests	Humidity [%]
C1	74.2
C2	73.5
N1	71.6
N4	69.7
N6	66.4
F1	73
F5	75.3

In average the humidity content was ~75 %. The most significant influence was that of the reaction pH. In this case, the higher the pH the lower the humidity of the $Mg(OH)_2$ cake.

A.5. $Mg(OH)_2$ suspensions magma density

The concentration of particles in a suspension is an important parameter that can influence settling and filtration properties. Table A2 lists magma density, Eq. (5), $M_{TMg(OH)_2}$, values of $Mg(OH)_2$ suspensions produced in the present work evaluated before and after settling.

Table A2
$Mg(OH)_2$ magma densities, Eq. (5), before and after settling, see Table 2 for further details.

Tests	$M_{TMg(OH)_2}$ [g/L] before settling	$M_{TMg(OH)_2} \cdot FC$ [g/L] after settling
C1	3.2 ± 0.1	53.6 ± 0.5
C2	3.2 ± 0.1	40.2 ± 0.5
N1	2.5 ± 0.1	42.0 ± 0.5
N2	2.9 ± 0.1	48.3 ± 0.5
N3	3.1 ± 0.1	52.3 ± 0.5
N4	3.4 ± 0.1	57.0 ± 0.5
N5	3.3 ± 0.1	41.6 ± 0.5
N6	3.2 ± 0.1	32.4 ± 0.5
F1	3.2 ± 0.1	79.9 ± 0.5
F5	3.2 ± 0.1	45.6 ± 0.5

Data availability

Data will be made available on request.

References

[1] U. Nations, Global issues water. https://www.un.org/en/global-issues/water. (Accessed 10 February 2025).
[2] M. Ayaz, M.A. Namazi, M.A. ud Din, M.I.M. Ershath, A. Mansour, el H.M. Aggoune, Sustainable seawater desalination: current status, environmental implications and future expectations, Desalination 540 (2022) 116022, https://doi.org/10.1016/j.desal.2022.116022.
[3] A. Ali, Z. Ali, U.M. Quraishi, A.G. Kazi, R.N. Malik, H. Sher, A. Mujeeb-Kazi, Integrating physiological and genetic approaches for improving drought tolerance in crops, in: Emerg. Technol. Manag. Crop Stress Toler, Elsevier Inc., 2014, pp. 315–345, https://doi.org/10.1016/B978-0-12-800875-1.00014-4.
[4] E. Jones, M. Qadir, M.T.H. van Vliet, V. Smakhtin, S. mu Kang, The state of desalination and brine production: a global outlook, Sci. Total Environ. 657 (2019) 1343–1356, https://doi.org/10.1016/j.scitotenv.2018.12.076.
[5] P. Loganathan, G. Naidu, S. Vigneswaran, Mining valuable minerals from seawater: a critical review, Environ. Sci.: Water Res. Technol. 3 (2017) 37–53, https://doi.org/10.1039/c6ew00268d.
[6] A. Shahmansouri, J. Min, L. Jin, C. Bellona, Feasibility of extracting valuable minerals from desalination concentrate: a comprehensive literature review, J. Clean. Prod. 100 (2015) 4–16, https://doi.org/10.1016/j.jclepro.2015.03.031.
[7] B.A. Sharkh, A.A. Al-Amoudi, M. Farooque, C.M. Fellows, S. Ihm, S. Lee, S. Li, N. Voutchkov, Seawater desalination concentrate—a new frontier for sustainable mining of valuable minerals, Npj Clean Water. 5 (2022), https://doi.org/10.1038/s41545-022-00153-6.
[8] S. Kim, E. Koh, M.J. Kim, Recovery of high-purity hydromagnesite from seawater through carbonation using Ca(OH)2, Desalination 586 (2024), https://doi.org/10.1016/j.desal.2024.117907.
[9] A.A. Pilarska, Ł. Klapiszewski, T. Jesionowski, Recent development in the synthesis, modification and application of Mg(OH)2 and MgO: a review, Powder Technol. 319 (2017) 373–407, https://doi.org/10.1016/j.powtec.2017.07.009.
[10] A. Kumar, G. Naidu, H. Fukuda, F. Du, S. Vigneswaran, E. Drioli, J.H. Lienhard, Metals recovery from seawater desalination brines: technologies, opportunities, and challenges, ACS Sustain. Chem. Eng. 9 (2021) 7704–7712, https://doi.org/10.1021/acssuschemeng.1c00785.
[11] Critical Raw Materials Resilience: Charting a Path Towards Greater Security and Sustainability. https://eur-lex.europa.eu/legal-content/EN/TXT/PDF/?uri=CELEX:52020DC0474&from=EN, 2020.
[12] G. Balducci, L. Bravo Diaz, D.H. Gregory, Recent progress in the synthesis of nanostructured magnesium hydroxide, CrystEngComm 19 (2017) 6067–6084, https://doi.org/10.1039/c7ce01570d.
[13] B. Sun, Y. Li, H. Guo, X. Chen, J. Cao, Fast and complete recovery of magnesium from sea bittern to synthesize magnesium hydroxide hexagonal nanosheet for enhanced flame retardancy and mechanical properties of epoxy resin, Desalination 583 (2024), https://doi.org/10.1016/j.desal.2024.117716.
[14] M.H. Gong, M. Johns, E. Fridjonsson, P. Heckley, Magnesium recovery from desalination brine, CEED Semin. Proc. (2018) 49–54.
[15] G. Battaglia, L. Ventimiglia, F. Vicari, A. Tamburini, A. Cipollina, G. Micale, Characterization of Mg(OH)2 powders produced from real saltworks bitterns at a pilot scale, Powder Technol. 443 (2024), https://doi.org/10.1016/j.powtec.2024.119918.
[16] M. Ahmed, A. Arakel, D. Hoey, M.R. Thumarukudy, M.F.A. Goosen, M. Al-Haddabi, A. Al-Belushi, Feasibility of salt production from inland RO desalination plant reject brine: a case study, Desalination 158 (2003) 109–117, https://doi.org/10.1016/S0011-9164(03)00441-7.
[17] C. Morgante, F. Vassallo, D. Xevgenos, A. Cipollina, M. Micari, A. Tamburini, G. Micale, Valorisation of SWRO brines in a remote island through a circular

approach: techno-economic analysis and perspectives, Desalination 542 (2022), https://doi.org/10.1016/j.desal.2022.116005.
[18] M. Micari, M. Moser, A. Cipollina, A. Tamburini, G. Micale, V. Bertsch, Towards the implementation of circular economy in the water softening industry: a technical, economic and environmental analysis, J. Clean. Prod. 255 (2020), https://doi.org/10.1016/j.jclepro.2020.120291.
[19] European Union, Hydroxide and peroxide of magnesium imports by country in 2023. https://wits.worldbank.org/trade/comtrade/en/country/EUN/year/2023/tradeflow/Imports/partner/ALL/product/281610. (Accessed 10 April 2025).
[20] M. Turek, W. Gnot, Precipitation of magnesium hydroxide from brine, Ind. Eng. Chem. Res. 34 (1995) 244–250, https://doi.org/10.1021/ie00040a025.
[21] H. Dong, C. Unluer, E.H. Yang, A. Al-Tabbaa, Synthesis of reactive MgO from reject brine via the addition of NH4OH, Hydrometallurgy 169 (2017) 165–172, https://doi.org/10.1016/j.hydromet.2017.01.010.
[22] C. Morgante, F. Vassallo, G. Battaglia, A. Cipollina, F. Vicari, A. Tamburini, G. Micale, Influence of operational strategies for the recovery of magnesium hydroxide from brines at a pilot scale, Ind. Eng. Chem. Res. 61 (2022), https://doi.org/10.1021/acs.iecr.2c02935.
[23] C. Morgante, F. Vassallo, C. Cassaro, G. Virruso, D. Diamantidou, N. Van Linden, A. Trezzi, C. Xenogianni, R. Ktori, M. Rodriguez, G. Scelfo, S. Randazzo, A. Tamburini, A. Cipollina, G. Micale, D. Xevgenos, Pioneering minimum liquid discharge desalination: a pilot study in Lampedusa Island, Desalination 581 (2024), https://doi.org/10.1016/j.desal.2024.117562.
[24] G. Battaglia, L. Ventimiglia, F. Vicari, A. Tamburini, A. Cipollina, G. Micale, Characterization of Mg(OH)2 powders produced from real saltworks bitterns at a pilot scale, Powder Technol. 443 (2024) 119918, https://doi.org/10.1016/j.powtec.2024.119918.
[25] D. Fontana, F. Forte, M. Pietrantonio, S. Pucciarmati, C. Marcoaldi, Magnesium recovery from seawater desalination brines: a technical review, Environ. Dev. Sustain. 25 (12) (2022) 13733–13754, https://doi.org/10.1007/s10668-022-02663-2.
[26] Y. Sano, Y. Hao, F. Kuwahara, Development of an electrolysis based system to continuously recover magnesium from seawater, Heliyon 4 (2018) 923, https://doi.org/10.1016/j.heliyon.2018.
[27] F. Vassallo, D. La Corte, A. Cipollina, A. Tamburini, G. Micale, High purity recovery of magnesium and calcium hydroxides from waste brines, Chem. Eng. Trans. 86 (2021) 931–936, https://doi.org/10.3303/CET2186156.
[28] R. Molinari, A.H. Avci, P. Argurio, E. Curcio, S. Meca, M. Plà-Castellana, J. L. Cortina, Selective precipitation of calcium ion from seawater desalination reverse osmosis brine, J. Clean. Prod. 328 (2021), https://doi.org/10.1016/j.jclepro.2021.129645.
[29] L. Ventimiglia, V.P. Atria, G. Battaglia, F. Vassallo, F. Vicari, A. Cipollina, G. Micale, A. Tamburini, Magnesium hydroxide production at a pilot scale: exploitation of different Mg2+-containing solutions, in: Lect. Notes Civ. Eng, 2024, pp. 187–191, https://doi.org/10.1007/978-3-031-63353-9_33.
[30] D. Pastorelli, D. Baaklini, A. Cipollina, G. Micale, A. Tamburini, M. Papapetrou, M. Bevacqua, F. Vicari, Method and installation for producing desalted and mineralized water from saline water, EP 4 112 567 A1, 2021.
[31] G. Virruso, C. Cassaro, F. Vassallo, A. Filingeri, A. Pellegrino, A. Tamburini, A. Cipollina, G.D.M. Micale, A pilot plant investigation on a real seawater brine valorisation via electrodialysis with bipolar membranes, J. Water Process Eng. 69 (2025) 106741, https://doi.org/10.1016/j.jwpe.2024.106741.
[32] M. Bevacqua, F. Vassallo, A. Cipollina, G. Micale, A. Tamburini, M. Papapetrou, F. Vicari, Rector and process for the precipitation of a solid product. https://worldwide.espacenet.com/patent/search/family/077126992/publication/WO2022238913A1?q=pn%3DWO2022238913A1, 2022.
[33] R. Turton, J.A. Shaeiwitz, D. Bhattacharyya, W.B. Whiting, Analysis, Synthesis and Design of Chemical Processes, Fourth, 2014.
[34] I.S. Fernandes, M.G. Domingos, M.F. Costa, R.J. Santos, J.C.B. Lopes, Hydrate-based desalination process using CO2 as hydrate forming agent – modelling and techno-economic analysis, Desalination 599 (2025), https://doi.org/10.1016/j.desal.2024.118426.
[35] EUROSTAT, Italy, Electricity prices: Non-household, medium size consumers. https://tradingeconomics.com/italy/electricity-prices-non-household-medium-size-consumers-eurostat-data.html. (Accessed 12 April 2025).
[36] V. Agmo Hernández, An overview of surface forces and the DLVO theory, ChemTexts 9 (4) (2023) 10, https://doi.org/10.1007/s40828-023-00182-9.
[37] A. Roa, J. López, G. Battaglia, A. Cipollina, J.L. Cortina, Integration of layer-by-layer hollow-fibre nanofiltration membranes and crystallization for water reclamation and resource recovery from acidic mine waters, Desalination 590 (2024), https://doi.org/10.1016/j.desal.2024.117960.
[38] G. Battaglia, S. Romano, A. Raponi, D. Marchisio, M. Ciofalo, A. Tamburini, A. Cipollina, G. Micale, Analysis of particles size distributions in Mg(OH)2 precipitation from highly concentrated MgCl2 solutions, Powder Technol. 398 (2022), https://doi.org/10.1016/j.powtec.2021.117106.
[39] M.A. Shand, The Chemistry and Technology of Magnesia, Wiley-Interscience, 2006.
[40] M. Del Mar De La Fuente García-Soto, E.M. Camacho, Boron removal by means of adsorption with magnesium oxide, Sep. Purif. Technol. 48 (2006) 36–44, https://doi.org/10.1016/j.seppur.2005.07.023.
[41] Magnifin H10. https://www.huberadvancedmaterials.com/solutions/products-brands/magnesium-hydroxide/magnifin.
[42] H. Dong, C. Unluer, E.H. Yang, A. Al-Tabbaa, Recovery of reactive MgO from reject brine via the addition of NaOH, Desalination 429 (2018) 88–95, https://doi.org/10.1016/j.desal.2017.12.021.
[43] Lafuente B. Downs R. T. Yang H. Stone N. n.d. The power of databases: the RRUFF project.
[44] X.F. Wu, G.S. Hu, B.B. Wang, Y.F. Yang, Synthesis and characterization of superfine magnesium hydroxide with monodispersity, J. Cryst. Growth 310 (2008) 457–461, https://doi.org/10.1016/j.jcrysgro.2007.10.025.